IL-27 limits HSPC differentiation during infection and protects from stem cell exhaustion

Daniel L. Aldridge[1], Zachary Lanzar[1], Anthony T. Phan[1], David A. Christian[1], Ryan Pardy[1], Booki Min[2], Ross M. Kedl[3], Christopher A. Hunter[1]

[1]University of Pennsylvania School of Veterinary Medicine, Philadelphia, PA, USA

[2]Department of Microbiology and Immunology, Feinber School of Medicine, Northwestern University, Chicago, IL, USA

[3]University of Colorado, Anschuitz Medical Campus, Aurora, CO, USA

Abstract

Many inflammatory stimuli can induce progenitor cells in the bone marrow to produce increased numbers of myeloid cells as part of the process of emergency myelopoiesis. These events are associated with innate training and can have long-term impacts on hematopoietic stem and progenitor cell (HSPC) development but can also compromise their function. While many cytokines support emergency myelopoiesis, less is known about the mechanisms that temper these events. When mice that lack the cytokine IL-27 were infected with *Toxoplasma gondii*, there was enhanced generation of monocyte progenitors and increased numbers of inflammatory monocytes. In the bone marrow of infected mice there was increased production of IL-27 that localized with HSPCs and a survey of cytokine receptor expression highlighted that HSPCs were uniquely poised to respond to IL-27. Furthermore, the use of *in vitro* differentiation assays and mixed bone marrow chimeras revealed that HSPCs from IL-27 deficient mice are pre-disposed towards the monocyte lineage. Additional studies highlighted that after infection loss of the IL-27R resulted in reduced HSPC fitness that manifested as reduced proliferative responses and a decreased ability to reconstitute the hematopoietic system. Thus, the ability of IL-27 to act on HSPC provides a regulatory brake on differentiation to limit monocyte induction and preserve HSPC stemness.

Introduction

In response to inflammatory stimuli, cytokine production can directly affect progenitor populations in the bone marrow leading to alterations in hematopoiesis (Collins et al., 2021). For example, in response to microbial challenges, elevated levels of GM-CSF, IFN-γ, and IL-6 can modulate hematopoietic stem and progenitor cell (HSPC) differentiation and enhance myelopoiesis (Baldridge et al., 2010; Kaufmann et al., 2018; Khan et al., 2020; Link, 2000; MacNamara et al., 2011a; MacNamara et al., 2011b; Maeda et al., 2005; Matatall et al., 2014; Miner et al., 2021; Mirantes et al., 2014; Reynaud et al., 2011). These events can also lead to long-term epigenetic and metabolic changes in HSPCs that form the basis for the process of innate training (Ochando et al., 2023). Thus, many of the cytokines produced during different infections are associated with innate training (Kaufmann et al., 2018; Khan et al., 2020). For example, after challenge with *Mycobacterium avium* or SARS-COV-2, IFN-γ and IL-6, respectively, can skew HSPCs towards myeloid output and increase the functionality of their downstream progeny (Cheong et al., 2023; Matatall et al., 2014).

While innate training is associated with long-term changes to hematopoietic stem cells (HSC), inflammation can also reduce HSC functionality, which can manifest as decreased proliferative and differentiation potential. To mitigate these adverse effects, there are cell-intrinsic mechanisms such as autophagic processes to limit oxidative damage, epigenetic reprogramming, and metabolic changes that contribute to the maintenance of stemness (Ibneeva et al., 2024; Liu et al., 2020; Ma et al., 2020; Revuelta and Matheu, 2017; Singh et al., 2018; Zhao and Deininger, 2023). Without these protective mechanisms, HSCs accumulate cellular damage and lose their ability to self-renew and differentiate, a process termed stem cell exhaustion. While inflammation is linked to HSC exhaustion, less is known about the cell extrinsic factors that contribute to the

56 maintenance of HSC quiescence and integrity, but several cytokines have been implicated in this
57 process. For example, in response to repeated stimulation with poly I:C, IFN-α can remove actively
58 proliferating HSCs from the developmental pool as a mechanism to prevent the accumulation of
59 damaged HSCs (Pietras et al., 2014). In addition, during fetal development there is evidence that
60 IL-10 limits HSC responsiveness to inflammatory signaling and thereby limit emergency
61 myelopoiesis as a mechanism to preserve HSC functionality (Collins et al., 2024).

62 IL-27 is a member of the Type I family of cytokines that utilize JAK-STAT signaling to
63 mediate their biological effects. This family also includes IL-6, and both of these cytokines signal
64 through dimeric receptors that contain the gp130 receptor combined with unique IL-6Rα and IL-
65 27Rα components. Because T cells constitutively express high levels of the IL-27R (Pflanz et al.,
66 2004; Pflanz et al., 2002), the majority of studies on this cytokine have focused on its impact on
67 these populations. Thus, IL-27 can limit the development of pathological Th1, Th2, and Th17
68 $CD4^+$ T cell responses (Findlay et al., 2010; Hamano et al., 2003; Villarino et al., 2003), but several
69 studies have also indicated that the absence IL-27 results in an elevated population of inflammatory
70 monocytes that contribute to the development of immune pathology (Aldridge et al., 2024; Liu et
71 al., 2021). The observation that the loss of IL-27 also results in enhanced inflammatory monocyte
72 induction prior to a detectable T cell response suggests that IL-27 may antagonize the innate
73 events that promote these monocyte populations (Aldridge et al., 2024). Consistent with this
74 idea, there are additional reports that IL-27 can limit neutrophil and monocyte responses
75 and directly impact myelopoiesis (Furusawa et al., 2016; Liu et al., 2014; Liu et al., 2021; Seita
76 et al., 2008; Sun et al., 2017; Wirtz et al., 2006). However, the observation that monocytes do not
77 express the IL-27R suggests that the ability of IL-27 to modulate this population is indirect.

78 The studies presented here show that infection with *T. gondii* results in increased HPSC
79 activity associated with emergency myelopoiesis; however, in the absence of IL-27, HSPCs
80 display a skewed developmental program that resulted in enhanced monopoiesis. While HSPCs
81 showed preferential expression of the IL-27R, the loss of IL-27 during infection resulted in reduced
82 HSPC fitness. Thus, during infection, the ability of IL-27 to act on HSPC provides a regulatory
83 brake on differentiation to limit monocyte induction and preserve HSPC stemness.
84

85 **Materials and Methods**

86 **Mice and infection**

87 Female and male C57BL/6 mice were purchased (8-12 weeks old; strain # 000664) from
88 Jackson labs as age and sex matched controls for whole body knockout mice. CD45.1 donor mice
89 were either bred in house or purchased from Jackson labs (10-12 weeks old; strain # 033076).
90 CD45.2 recipient mice were purchased from Taconic labs (10-12 weeks old; model # B6-M). IL-
91 27R$^{-/-}$ (Jackson labs; strain # 018078) were bred in house, as were IL-27p28$^{-/-}$ mice, originally
92 generated by Lexicon Pharmaceuticals, Inc. and previously described (Hall et al., 2012). IL-27-
93 p28-GFP reporters (Kilgore et al., 2018) were similarly bred in house, and the Procr-Ai6 was
94 generated from crossing the Procr-ERT2-cre line (Procr: Jacson labs; strain # 033052) which had
95 been backcrossed 9 generations onto the C57BL/6 background and was provided by Dr. Nancy
96 Speck to the Ai6 mouse line (Jackson labs; strain# 007906). Mice that contain a floxed allele of
97 the IL-27Rα (IL-27R$^{fl/fl}$) were provided by Dr. Booki Min (Do et al., 2017), and maintained within
98 our mouse colony. This line was then crossed with a CD4-cre mouse (Jackson labs; strain# 022071)
99 to generate the CD4^{cre}-IL-27R$^{flox/flox}$ mouse line. M1Red mice, which express red fluorescent
100 protein (RFP, encoded by *dsRed2*) under control of the *Irgm1* promoter, were received from

101 Gregory Taylor (Duke University) and maintained in-house. All mice were housed and bred in
102 specific pathogen-free (SPF) facilities in the Department of Pathobiology at the University of
103 Pennsylvania in accordance with institutional guidelines (IACUC# 805045). Cysts of ME49 strain
104 of *T. gondii* were collected from chronically infected CBA mice brain tissues. Experimental mice
105 were then infected i.p. with 20 cysts. For experiments where uninfected bone marrow was sorted,
106 a Prugniaud (PRU) strain of *T. gondii* expressing tdTomato was used (Pru-tdTomato). Both of
107 these are type II strains and show similar virulence.
108
109 **Functional Analysis of HSPC *in vivo***
110 For induction of the Procr-ERT2-cre, tamoxifen was given for three consecutive days (5
111 mg/mouse) prior to infection. For BRDU proliferation labeling, 5 mg of BRDU was given i.p. to
112 each mouse the same day as infection. 1mg/ml of BRDU was then provided in the drinking water
113 to mice throughout infection. To generate bone marrow chimeras, recipient mice were given a
114 radiation dose of 900-1000 rads at least 6 hrs. prior to transferring donor marrow. Donor marrow
115 was transferred (at least $2x10^6$ cells from each donor, unless otherwise stated; this resulted in a
116 total of $4x10^6$ cells being transferred for mixed chimeras) intravenously (i.v.) via retro-orbital
117 injection. Mice were then given 5 mL of Sulfamethoxazole/ Trimethoprim (200mg+40mg/5ml) in
118 their drinking water and replaced every 2-3 days for two weeks.
119
120 **Cell staining, flow cytometry, UMAP analysis, and detection of IL-27**
121 Splenocytes were obtained by grinding spleens through a 70 μm filter and washing with
122 RPMI supplemented with 5% fetal bovine serum (FBS). Red blood cells were then lysed by
123 incubating samples with ACK lysis buffer (Thermo Fischer Scientific) for 5 minutes before

124 washing again with RPMI + 5% FBS. Both femurs and tibias were harvested from mice for bone
125 marrow isolation. Connective tissue was removed from the bones by gentle scraping with a scalpel
126 before one end of each bone was cut off to expose the marrow. Bones were then placed in a 0.5 ml
127 microcentrifuge tube, with a hole punctured in the bottom with a 31g needle. The 0.5ml tube was
128 then placed within a 1.5 ml microcentrifuge tube; the nested tubes were then spun down at 13, 000
129 rcf for 1.5 min. The pelleted cells were then ACK lysed and washed as above (centrifuging at 500
130 rcf) before being passed through a 70 µm strainer and resuspended in appropriate media (adapted
131 from (Au - Amend et al., 2016)). For peritoneal exudate cells (PECs), 8 mL of PBS was injected
132 into the peritoneum of mice (21G needle attached to a 10 mL syringe) and re-aspirated using the
133 same needle and syringe. Syringe contents were then expelled into a 15 mL conical tube, spun
134 down at 300 rcf, and resuspended in appropriate media.

135 After cell numbers were determined for each sample, equivalent numbers of cells were
136 plated in a 96-well plate and spun down at 300 rcf. Cells were then washed with FACS Buffer [1x
137 PBS, 0.2% bovine serum antigen, 1mM EDTA] before incubating with Fc block [99.5 % FACS
138 Buffer, 0.5% normal rat serum, 1 µg/ml 2.4G2 IgG antibody] prior to staining. If CD16/32 was
139 stained for, the staining antibody was substituted for unconjugated 2.4G2 antibody in the Fc block.
140 Cells were stained with the viability dye Ghost Dye Violet 510 (Tonbo biosciences; 12-0870), and
141 the following antibodies were used for subsequent staining: CD90.2 (BD; clone 30-H12), B220
142 (BD; clone RA3-6B2), Ly6G (BD; clone 1A8), CD11b (BD; clone M1/70), Ly6C (Biolegend;
143 clone HK1.4), Sca-1 (BD/Invitrogen; clone D7), CD117/cKit (Biolegend; clone ACK2), CD135
144 (Biolegend; clone A2F10), CD150 (Biolegend; clone TC15-12F12.2), CD48 (Biolegend/BD;
145 clone HM48-1), CD127 (Biolegend; clone A7R34), CD16/32 (BD; clone 2.4G2), CD34
146 (Invitrogen; clone RAM34), CD115 (Biolegend; clone AFS98), CCR2 (Biolegend; clone

147 SA203G11), CX3CR1 (Biolegend; clone SA011F11), CD11c (Biolegend; clone N418), XCR1
148 (Biolegend; clone ZET), CD172a (Biolegend; clone P84), CD64 (Biolegend; clone X54-5/7.1),
149 F4/80 (Invitrogen; clone BM8), MHCII (Biolegend; clone M5/114.15.2), gp130 (Biolegend; clone
150 4H1B35), IL-27Rα (BD; 2918), CD132 (BD; clone 4G3), CD131 (BD; clone JORO50), IL-6Rα
151 (Biolegend; clone D7715A7), GM-CSFRα (R&D systems; clone 698423), CD210/IL-10R
152 (Biolegend; clone 1B1.3a), IFN-γR β (Biolegend; clone MOB-47), IFNAR-1 (Biolegend; clone
153 MAR1-5A3), IL-21R (Biolegend; clone 4A9), CD120a/TNFRI (Biolegend; clone 55R-286),
154 CD120b/TNFRII (Biolegend; clone TR75-89), and CD217/IL-17RA (Biolegend; clone
155 S19010F).

156 Intracellular staining for Ki67 (BD; clone B56), and BCL2 (Biolegend; clone BCL/10C4)
157 was performed using the Foxp3/Transcription Factor Staining Buffer Set (eBioscience) according
158 to the manufacturer's instructions. BRDU staining was done following a previous published
159 protocol (Matatall, Methods Mol. Biol., 2018). Cells within the vasculature were labeled by
160 injecting 3 μg of florescent anti-CD45 antibody (Biolegend; clone 30-F11)/mouse for 3 min prior
161 to euthanasia. Samples were run on a FACSymphony A3 or A5 (BD) and analyzed using the
162 FlowJo Software analysis program (TreeStar). For UMAP analyses, either 500 or 10,000 live cells
163 (for 5 days of culture or 10, respectively) per sample were sampled using the downsampling plug-
164 in (TreeStar) and subsequently concatenated. The concatenated samples were then used for UMAP
165 analysis with the FlowJo plug-in (TreeStar), using Euclidean distances with the nearest neighbor
166 set to 15, minimum distance of 0.5, and number of components set to 2. All compensated
167 parameters were then used in the analysis. After the UMAP analysis was performed, the X-shift
168 plug-in (TreeStar) was used to further analyze each cluster for its defining features (Samusik et al.,
169 2016).

170 For IL-27p28 detection, mouse IL-27p28/IL-30 Quantikine ELISA kit (M2728; R&D
171 Systems) was used according to the manufacturer's protocol.
172
173 **Immunofluorescence of bone marrow and image analysis**
174 Procr^{tdTomato}IL-27p28^{GFP} mice were generated, infected, and long bones harvested at 5 dpi.
175 The bones were then fixed in 4 % PFA for 2.5-4 hrs, washed with PBS 3x, and then decalcified in
176 0.5mM EDTA for ≥72 hrs before being paraffin embedded. 5 µm sections were taken and placed
177 onto charged microscope slides. For staining, slides were de-paraffinized, rehydrated, and placed
178 in 1mM EDTA (pH 8.0) overnight in a 55°C water bath to recover epitopes prior to staining. Slides
179 were washed in diH_2O the next day before proceeding with staining. Staining was adapted from
180 (Im et al., 2019). Slides were blocked with 100µl of blocking buffer (1x PBS+0.3% triton X-
181 100+1:200 rat IgG) for 30 min at room temperature. Slides were then washed 3x, for 5 min each
182 with PBS. Endogenous streptavidin and biotin were then blocked using the ReadyProbes
183 Stretavidin/Biotin Blocking solution (Invitrogen) according to the manufacturer's directions. After
184 washing, GFP was stained for at 1:40 with anti-GFP AF488 (Biolegend; FM264G) overnight at
185 4°C. Slides were washed 3x with PBS, as above, and then mounted and coverslipped using 15µl
186 Fluoro-Gel (Electron Microsopy Sciences). Slides were then imaged on a Stellaris Falcon (Leica)
187 microscope.
188 Images were processed and analyzed using the Fiji software package (Schindelin et al.,
189 2012). Images were converted to binary images, manually thresholded, watersheding applied to
190 separate overlapping objects, and positive cells counted using the "analyze particles" tool.
191
192 **Statistics**

193 An unpaired, Welch's t-test or one-way ANOVA with Sidak's correction for multiple
194 comparisons were used to test for significant differences between groups. These were used as
195 indicated in each figure and unless otherwise stated. P values of less that 0.05 were considered
196 significant.
197
198
199 **Results**
200 **IL-27 regulates monopoiesis during toxoplasmosis**
201 Infection with *T. gondii* leads to increased production of monocytes that is enhanced in the
202 absence of IL-27 (Aldridge et al., 2024), but it is unclear if this is a result of differentiation from
203 HSPCs or from the more differentiated monocyte progenitors (MPs). Therefore, the Procr-ERT2-
204 cre mouse line, which expresses Cre in HSPCs (Gur-Cohen et al., 2015; Iwasaki et al., 2010), was
205 crossed with the Ai6 reporter line to provide a lineage tracing model. In these mice, tdTomato is
206 expressed in *procr*$^+$ cells and, upon tamoxifen (TAM) treatment, HSPCs will be tdTomato$^+$ and
207 GFP$^+$ but their differentiated progeny will only express zsGreen (Fig. 1A). For these experiments,
208 Procr-Ai6 mice were treated with TAM, infected, and then at 5 dpi the BM and peripheral cells
209 were analyzed. Consistent with other HSPC lineage tracing models (Chapple et al., 2018; Säwen
210 et al., 2018), in naïve bone marrow only a small proportion (~5%) of long-term hematopoietic
211 stem cells (LTHSCs) were labeled which corresponded to a low proportion of zsGreen$^+$ monocytes
212 in the peritoneum and spleen (Fig. 1B-C). After infection, the proportion of zsGreen$^+$ LTHSCs in
213 the marrow nearly doubled (Fig. 1B), and the proportion of monocyte dendritic cell progenitors
214 (MDP) also increased (Supp Fig. 1A). This corresponded to an increase in labeled monocytes and
215 neutrophils in the bone marrow of infected mice (Supp. Fig. 1A). In the periphery, there was also

216 an increased proportion of zsGreen^{+} monocytes in the spleen, and the proportion of labeled
217 monocytes in the peritoneum, the site of initial infection, reached 100% (Fig. 1C). These
218 progenitors and their progeny were defined based on the expression of defining surface markers
219 as measured by flow cytometry (Supp. Fig. 2). Additional phenotyping revealed that both classical
220 (CCR2^{hi}, CX3CR1^{lo}) and non-classical (CCR2^{lo}, CX3CR1^{hi}) monocyte population were labeled to
221 equivalent degrees, indicating that infection impacts the recruitment of both subsets (Supp. Fig
222 1B). These data sets indicate that the increased myelopoiesis that occurs in response to infection
223 with *T. gondii* is due to expansion and enhanced differentiation of HSPCs, and not just MPs, into
224 downstream progeny, eventually resulting in increased monocyte production.

225 To determine the impact of IL-27 on this infection induced myelopoiesis, WT and IL-
226 27p28$^{-/-}$ mice were challenged with *T. gondii* and numbers of progenitors (from LTHSCs to MPs)
227 were analyzed (Fig. 1D). While infection led to an expansion of LTHSCs, the numbers of LTHSC,
228 granulocyte progenitors (GP), and other HSPCs (including common lymphocyte progenitors
229 (CLPs), common myeloid progenitors (CMPs), and granulocyte monocyte progenitors (GMPs))
230 (data not shown) were not impacted by the absence of IL-27 (Fig. 1E). Infection also resulted in
231 a transient increase in MPs in WT mice, but in the absence of IL-27 this was enhanced at 3 and 5
232 dpi before returning to baseline at 10 dpi (Fig. 1F). A similar pattern was observed for the MDPs
233 (Supp. Fig. 1C), and in the IL-27p28$^{-/-}$ mice this corresponded to an increase in mature monocytes
234 in the liver (Supp. Fig. 1D). The CCR2^{hi}CX3CR1^{lo} phenotype of these cells indicated that these
235 were inflammatory monocytes, that were predominantly within the tissue parenchyma (Supp. Fig.
236 1E), suggesting that these monocytes are poised to participate in the tissue pathology associated
237 with these mice. Thus, one function of IL-27 during acute toxoplasmosis is to limit monopoiesis
238 and the generation of inflammatory monocytes.

239

240 **IL-27 regulates monocyte development in a cell intrinsic manner**

241 Previous studies have shown that during toxoplasmosis or trypanosomiasis the absence of
242 IL-27 results in enhanced $CD4^+$ T cell responses which contribute to increased accumulation of
243 inflammatory monocytes (Aldridge et al., 2024; Liu et al., 2021). To test if the early (5 dpi)
244 enhanced monopoiesis in the IL-$27^{-/-}$ mice observed here was a secondary consequence of the
245 $CD4^+$ T cell response, a $CD4^{cre}$ IL-$27R^{fl/fl}$ (CD4-IL-27R) mouse line was generated. In these mice
246 IL-27R expression was efficiently deleted in T cells, but other IL-27R expressing cells, such as B
247 cells, maintained expression (Supp. Fig. 3A). When infected with *T. gondii* these mice
248 phenocopied whole body IL-$27R^{-/-}$ mice and developed lethal immune pathology > 10 days post-
249 infection (data not shown). When control and CD4-IL-27R mice were infected and analyzed at 5
250 dpi there were equivalent numbers of monocyte progenitors (Fig. 2A). Thus, the enhanced
251 monopoiesis observed in the whole-body IL-$27p28^{-/-}$ mice is independent of the effect of IL-27 on
252 $CD4^+$ T cells.

253 Next, a mixed bone marrow chimera approach was used to determine if the enhanced
254 monopoiesis observed in the absence of IL-27 was cell intrinsic. In these experiments, WT and IL-
255 $27R^{-/-}$ marrow from naïve mice was used to generate a series of individual and mixed bone marrow
256 chimeras (Fig 2B). In the single-transfer chimeras, at fourteen weeks after reconstitution WT and
257 IL-$27R^{-/-}$ marrow reconstituted the hematopoietic system of irradiated recipients with 100% of
258 hematopoietic cells derived from the donor (Supp. Fig. 3B-C, left bars). However, in the mixed
259 chimeras, $IL27R^{-/-}$ cells had a reduced engraftment of LTHSCs and generation of downstream MPs
260 (Supp. Fig. 3B, right bars, a 40:60 ratio KO: WT). Despite this reduction in the IL-$27R^{-/-}$ LTHSC
261 the population of $CCR2^{hi}CX3CR1^{lo}$ monocytes in the periphery were preferentially derived from

262 the IL-27R$^{-/-}$ lineage (Supp. Fig. 3C, right bars, 60:40 ratio KO:WT). To determine if infection
263 would impact this differentiation, these mixed chimeras were infected with *T. gondii* and analyzed
264 at 5 dpi (Fig. 2C). After infection, IL-27R$^{-/-}$ LTHSC remained deficient in the mixed chimeras, but
265 MPs from both lineages were equivalent (Fig. 2C, right bars). Additionally, the CCR2^{hi}CX3CR1^{lo}
266 monocytes were still predominately derived from the IL-27R$^{-/-}$ lineage (Fig. 2D, right bars).
267 Together, these data indicate that at homeostasis and during infection IL-27 can support LTHSC
268 populations but also temper the downstream processes that lead to monocyte production.
269 Additionally, this function is independent of IL-27 signals on CD4^{+} T cells, but rather is due to a
270 cell intrinsic ability of IL-27 to limit the production of inflammatory monocytes.
271
272 **IL-27p28 is expressed in the bone marrow at homeostasis and during infection**
273 Given the impact of IL-27 on myelopoiesis described above, studies were performed to
274 characterize the cellular sources of IL-27p28 and their spatial location in the bone marrow of naïve
275 and infected mice. WT mice were infected, bone marrow harvested at 0, 3, 5, and 10 dpi, and local
276 production of the IL-27p28 subunit assayed (Fig. 3A). At 0 dpi, low constitutive levels of IL-27p28
277 were detected and increased throughout infection, with a peak at 5 dpi and elevated levels
278 maintained at 10 dpi (Fig. 3A). The use of an IL-27p28-GFP reporter mouse (Aldridge et al., 2024;
279 Kilgore et al., 2018) revealed a small population of p28-GFP^{+} cells in the bone marrow of naïve
280 mice, but by 5dpi this was expanded (Fig. 3B-C). Additional analysis of the bone marrow and
281 peripheral tissues (spleen, blood, PEC) (Fig. 3B-C) revealed that although a small proportion of T
282 cells were GFP^{+}, consistent with other reports (Kimura et al., 2016; Lin et al., 2023), monocytes
283 and macrophages were the dominant source of IL-27 in these sites, by proportion of GFP^{+} cells as
284 well as by cell number (Fig. 3B-C, Supp. Fig. 4A). Additionally, monocyte populations expressed

285 the highest levels of IL-27p28-GFP in comparison to other populations, such as dendritic cells
286 (Supp. Fig. 4B).

287 To visualize the spatial relationship between IL-27 expressing cells and HSPCs, femurs
288 from naive IL-27p28-GFP mice and imaged. In naïve mice, a stain for Sca-1 revealed low numbers
289 of HSPCs while $p28^{GFP+}$ cells were present at a higher frequency; however, few of the cells in each
290 population colocalized (Supp. Fig. 4C, yellow arrows). During infection the expression of Sca-1
291 is upregulated by many cell populations (Baldridge et al., 2011; Morales-Mantilla et al., 2022),
292 and so the $Procr^{tdTomato+}$ cre reporter mouse (identifying HSPCs) was crossed with the IL-$27p28^{GFP}$
293 reporter. As HSCs are typically found within the hypoxic regions of the bone marrow (Eliasson
294 and Jönsson, 2010; Parmar et al., 2007), i.v. injection of anti-CD31 was used to label arterioles to
295 distinguish regions of the marrow that are highly vascularized or more hypoxic.
296 Immunofluorescence of the femur from 5 dpi highlighted that, similar to flow cytometric analysis
297 of the BM of the IL-27p28 reporters, infection resulted in increased numbers of $p28^{GFP+}$ cells (Fig.
298 3D). $Procr^{tdtomato}$ had a homogenous distribution in the femur (Supp. Fig. 4D, middle) whereas
299 $p28^{GFP+}$ expression was more regional (Fig 3D; Supp. Fig. 4D, top). This was quantified by
300 sampling throughout the femur section (Fig 3D; Supp. Fig. 4D, regions 1-8). The area containing
301 almost exclusively $Procr^{tdTomato+}$ HSPCs, but few $p28^{GFP+}$ cells, was an area of low vascularization,
302 consistent with the HSC niche (Fig. 3D; Supp. Fig. 4D, regions 3-5). However, in regions close to
303 the $CD31^{+}$ vasculature, HSPCs and IL-$27p28^{+}$ cells were found in proximity to one another (Fig.
304 3D; Supp. Fig. 4D, regions 1-2 and 6-8). When these regions were grouped based on this
305 vascularization, and GFP expressing cells normalized to $tdTomato^{+}$ cells, a marked decrease in
306 GFP^{+} cells was apparent in hypovascularized regions (Fig. 3D). These data indicate that during

307 infection the p28-GFP$^+$ BM monocytes associate with HSPCs, and this is most apparent near the
308 vasculature and away from the HSC niche.
309
310 **Developmental expression of the IL-27R by hematopoietic cells**
311 The hematopoietic tree begins with undifferentiated LT-HSCs that differentiate into distinct
312 hematopoietic lineages and mature progeny; the color scheme in Fig. 4A reflects these
313 developmentally related populations. To determine which progenitor stages in the marrow were
314 responsive to IL-27, the expression of the IL-27Rα was compared with other cytokine receptors
315 (gp130, the IL-2R common gamma chain (CD132), IL-6Rα, and GM-CSFRα) that modulate
316 hematopoiesis (Collins et al., 2021; Reynaud et al., 2011). Expression of these receptors was
317 measured on HSPCs and committed progeny in naïve and infected mice (Fig. 4B-C; Fig. 5A-D).
318 The gp130 receptor, one chain of the IL-27 receptor that is also utilized by other IL-6 family
319 members, was expressed by all developmental stages examined in both naïve and infected mice
320 (Fig. 4B). In contrast, the IL-27Rα was highly expressed by LTHSCs, but markedly decreased
321 with lineage commitment, with mature neutrophils and monocytes showing no expression (Fig.
322 4C). The use of the Haemosphere RNA-seq data set (Choi et al., 2018) and the BloodSpot online
323 tool (Bagger et al., 2015) for the analysis of normal mouse hematopoietic bone marrow transcripts
324 (Chambers et al., 2007; Di Tullio et al., 2011) confirmed that levels of *IL27RA* mRNA were high
325 in LSKs and LTHSCs but decreased with lineage commitment (Supp. Fig. 5A-B). To determine
326 if IL-27R signaling was functional on HSPCs, bulk bone marrow was collected from M1Red
327 reporter mice (Pardy et al., 2024; Stifter et al., 2019), which express RFP under the control of the
328 *Irgm1* promoter, downstream of STAT1 signaling. When these cells were treated with IL-27 (an

329 activator of STAT1) the myeloid committed progenitors showed minimal RFP expression (Supp.
330 Fig. 5C), whereas HSPCS showed a time-dependent increase in reporter expression (Fig. 4D).
331 When expression of the common IL-2R gamma chain (utilized by IL-2, -4, -7, -9, -15, and
332 -21), was analyzed, like gp130, it was ubiquitously expressed by all developmental stages,
333 although infection did upregulate its expression (Fig. 5A). Similarly, CD131, which is shared by
334 GM-CSF, IL-3, and IL-5 signaling, was expressed in most developmental stages and was markedly
335 enhanced upon infection (Fig. 5B). In contrast to the IL-27Rα, the expression of IL-6Rα and GM-
336 CSFRα by HSPCs was negligible, and the highest expression of these was detected on fully
337 committed, mature neutrophils and monocytes (Fig. 5C-D). Additionally, both the IL-6Rα and
338 GM-CSFRα showed enhanced expression during infection, further differing from IL-27Rα. A
339 summary of the survey for IL-10R, IFNγRβ, IFNαR, IL-17Rα, TNFIR, and TNFIIR is presented
340 in Supp. Fig. 6, and highlights that while some of these were constitutively expressed across
341 the hematopoietic tree, none of these receptors showed preferential expression by HSPCs.
342 Thus, this survey of cytokine receptor expression highlights that HSPCs but not downstream
343 progenitors are uniquely positioned to respond to IL-27.
344
345 **Infection derived IL-27 restrains a monocytic differentiation program in HSPCs**
346 To determine the impact of infection-driven IL-27 on HSPC differentiation, LTHSCs were
347 sorted from naïve or infected WT and IL-27R$^{-/-}$ mice at 5 dpi (see Supp. Fig. 7 for gating strategy).
348 These LTHSCs were then cultured in MethoCult and their phenotype and ability to form colonies
349 was quantified by morphology after 5 or 10 days of culture (Supp. Fig. 8). As expected, cells from
350 naïve mice generated all colony types, but in cultures derived from infected mice there were
351 reduced granulocyte/monocyte (GM) and granulocyte (G) colonies (Supp. Fig. 8A). However, by

352 10 days post-culture (dpc), there was a slight enhancement in macrophage/monocyte colonies (M)
353 from infected mice. The significant loss of colonies from infected mice, though, made
354 quantification of these colonies difficult. Thus, to better quantify these differences these cultures
355 were analyzed by flow cytometry to measure expression of canonical developmental markers (see
356 materials and methods). Dimensional reduction was then performed via UMAP, and cluster
357 formation was analyzed with X-shift to determine the dominant markers associated with individual
358 clusters. When cells were concatenated from all collection timepoints, 14 clusters were delineated
359 (Supp. Fig. 8B). These clusters where driven, predominantly, by either collection time (Supp. Fig.
360 8B, top) or proliferative status (Supp. Fig. 8B, bottom). Clusters 1-9 contained only samples from
361 5 dpc, and clusters 1-6 corresponded to undifferentiated, quiescent colonies that were minimally
362 proliferative (Ki67^{lo}) while clusters 7-9 were starting to proliferate (Ki67^{hi}) and differentiate to
363 give rise to mature cell populations. By 10 dpc, there was a loss of the quiescent colonies and a
364 rise of populations (clusters 10-14) that are Ki67^{hi} but have increased expression of mature myeloid
365 markers (CD11b, CD16/32, and Ly6C) (Supp. Fig. 8C). This reflects the increased differentiation
366 of colonies into mature myeloid cells. The UMAP analysis highlighted clusters 1, 6, 7, and 14 as
367 the dominant output of this assay (Supp. Fig. 8D): Cluster 1-undifferentiated progenitors (Ki67^{lo},
368 BCL2^{mid}, no other expression), Cluster 6-myeloid biased HSPCs (CD150^{hi}), Cluster 7- monocyte
369 progenitors (intermediate expression of myeloid markers (CD16/32^{lo}) , but expression of
370 progenitor markers (CD34^{int})), and cluster 14-mature monocyte (CD11b^{hi}, Ly6C^{hi}, CD16/32^{int})
371 (Supp. Fig. 8C). Furthermore, this clustering analysis highlighted that infection resulted in a loss
372 of myeloid progenitors (cluster 7) that was further reduced in the absence of IL-27 (Supp. Fig. 8E).
373 However, by 10 dpc this corresponded to enhanced differentiation into mature monocytes (cluster
374 14).

375 To compare the ability of HSPCs from WT or IL-27R$^{-/-}$ mice to generate monocyte
376 populations, cells solely from 10 dpc were clustered (Fig. 6A), with the dominant clusters being
377 1, 2, 3, 10, and 11 (Fig. 6B). Of these, HSPCs were present in cluster 1 (Sca-1^{+}cKit/CD117^{+}),
378 while cluster 10 contained monocyte progenitors (CD11b^{hi}Ly6C^{low}CD34^{+}CD115^{+}), and cluster 11
379 expressed markers of mature monocytes (CD11b^{hi}Ly6C^{+}) (Fig. 6C-D). Further analysis (Fig. 6E),
380 revealed that HSPCs from infected mice produced increased numbers of monocytes and
381 macrophages (cluster 11), but only HSPCs from infected, IL-27R$^{-/-}$ mice were enhanced in their
382 differentiation into monocyte progenitors (cluster 10). Thus, during infection the loss of IL-27
383 signaling enhances the skewing of HSPCs *ex vivo* toward monocyte differentiation.
384 In a complimentary *in vivo* approach, HSPCs from naïve or infected WT or IL-27R$^{-/-}$ mice
385 were transferred into irradiated WT hosts and differentiation assessed (Fig. 6F). For these
386 experiments bulk marrow was utilized because, as discussed above, inflammation results in
387 upregulation of Sca-1 and other lineage defining markers (Baldridge et al., 2011; Morales-Mantilla
388 et al., 2022), making it difficult to define true HSPCs for transfer by cell-sorting. In addition, for
389 these studies mice were infected with a strain of *T. gondii* that expresses tdTomato (Pru-tdTomato)
390 (Christian et al., 2014; John et al., 2009) to allow parasite removal during sorting and prevent
391 infection of irradiated recipients. Analysis of spleens of recipient mice at 12 weeks, revealed that
392 donors from naive or infected IL-27R$^{-/-}$ mice produced more monocytes than those derived from
393 WT mice (Fig. 6F). These *ex vivo* and *in vivo* approaches indicate that exposure of LTHSCs to IL-
394 27 during infection results in a stable program that limits monocyte production.
395
396 **IL-27 regulates the functionality and fitness of HSPCs during infection**

397 While the data sets presented above indicate a role for IL-27 in the regulation of HSPC
398 differentiation, it was unclear if loss of IL-27 signals during infection would affect their
399 functionality and fitness. To test if there were alteration in HSPC proliferation during infection,
400 WT and IL-27R$^{-/-}$ mice were treated with BRDU throughout infection and HSPC proliferation
401 analyzed at 5 dpi. The combination of Ki67 expression and BRDU incorporation was used to
402 distinguish HSPCs entering cell cycle (Ki67^{+}BRDU^{-}), cells that have entered cell cycle and are
403 actively proliferating (Ki67^{+}BRDU^{+}), and those that have proliferated but are no longer in cell
404 cycle (Ki67^{-}BRDU^{+}). In WT mice, the majority of LSKs are quiescent (Ki67^{-}BRDU^{-}), a proportion
405 of cells have entered cell cycle (Ki67^{+} BRDU^{-}), and a distinct Ki67^{+}BRDU^{+} population, as well as
406 a smaller Ki67^{-}BRDU^{+} population, can be detected. In the absence of IL-27 signaling, the most
407 prominent difference was a reduced proportion of Ki67^{+}BRDU^{+} cells (Fig. 7A). To determine if
408 this decreased Ki67^{+}BRDU^{+} population might be due to increased cell death of HSPCs in the IL-
409 27R$^{-/-}$ mice, cells were stained for Annexin V and a free-amine reactive viability dye to
410 discriminate early- and late-apoptotic cells as well as necrotic cells. No difference in cell death
411 was observed between WT and IL-27R$^{-/-}$ HSPCs (Supp. Fig. 9A). These data need to be interpreted
412 with care, as total HSPC numbers are not different between WT and IL-27$^{-/-}$ mice (see Fig 1), but
413 they suggest that IL-27 may regulate either the proliferation or retention of HSPCs within the bone
414 marrow niche.

415 A key feature of healthy HSCs is their ability to reconstitute the hematopoietic system of
416 irradiated mice, even after serial transfer (Siminovitch et al., 1964; Weissman, 2000). However,
417 inflammation and over-proliferation of HSCs can impair their ability to rescue lethally irradiated
418 recipients (Feng et al., 2008; King et al., 2011; Pietras et al., 2014). To test the impact of IL-27 on
419 HSC fitness and functionality, serial transplantations of HSCs from infected WT and IL-27R$^{-/-}$

420 mice were performed. In these experiments, marrow from naïve or infected donors was used to
421 produce single chimeras or to provide a 1:1 mix of WT and IL-27R$^{-/-}$ populations that were
422 transferred to irradiated recipients (Fig. 7B). All transfers promoted host survival and at 9 weeks
423 post-transplantation, the WT or IL-27R$^{-/-}$ donors from naïve and infected mice reconstituted the
424 blood compartment with a similar efficiency (Supp. Fig. 9B). However, in the 1:1 chimeras from
425 infected mice, the peripheral compartment was dominated by cells derived from WT mice.
426 Analysis of the marrow of the single transfer chimeras at 12 weeks post-transplant highlighted that
427 when donor cells were derived from infected mice there was a significant reduction in the LTHSC
428 compartment (Fig. 7C). To test the functionality of these HSCs, they were then transplanted for a
429 second time into irradiated hosts (Fig. 7D). Mice that received a secondary transplant of marrow
430 from naïve WT and IL-27R$^{-/-}$ mice survived irradiation, consistent with the ability of healthy HSCs
431 to undergo at least three rounds of transplantation (Siminovitch et al., 1964; Weissman, 2000).
432 Additionally, secondary transplantation of WT HSCs from infected mice also resulted in survival
433 of these hosts. However, the serial transfer of marrow from infected IL-27R$^{-/-}$ mice did not save
434 irradiated recipients (Fig. 7D). Thus, while IL-27R$^{-/-}$ HSPCs from infected mice maintain a
435 differentiation bias towards the monocyte lineage, they have a decreased survival and proliferation
436 capacity and a reduced ability to rescue irradiated mice.
437

438 **Discussion**

439 During toxoplasmosis, the increased production of inflammatory monocytes is critical to
440 control infection (Dunay et al., 2008), but these populations also have regulatory properties that
441 help to limit immune-pathology. For example, as infection progresses, the presence of IFN-γ in the
442 bone marrow promotes the production of monocytes that produce IL-10 and PGE_2 (Askenase et

443 al., 2015) which contribute to the restoration of homeostasis. Similarly, during toxoplasmosis and
444 other infections in response to IFN-γ/STAT1 signals (Furusawa et al., 2016 and our own
445 unpublished observations) monocytes become a dominant source of IL-27 (Detavernier et al.,
446 2019; Hall et al., 2012). While IL-27 has a critical role in directly limiting pathological T cell
447 responses, the data presented here show that IL-27 is also part of a regulatory loop that acts on
448 HSPCs to limit emergency myelopoiesis. Infection-induced monopoiesis gives rise to a population
449 of IL-27^{+} monocytes in the bone marrow that can then act on HSPCs to limit further monocyte
450 production. This observation is reminiscent of reports that IFN-γ activated
451 monocytes/macrophages can directly limit HSPCs (McCabe et al., 2015; Seyfried et al., 2020) or
452 the ability of IL-10 to limit emergency myelopoiesis in the fetus (Collins et al., 2024).

453 One challenge that faces HSCs during inflammation is the need to protect from stressors
454 associated with proliferation that adversely affect the functions of these cells (Caiado et al., 2021).
455 The concept of HSC "exhaustion" has been developed to describe HSCs that are no longer able to
456 fulfill their role in proliferation and reconstitution of steady-state hematopoiesis (Singh et al., 2020;
457 Zhao and Deininger, 2023). Unanticipated findings from our studies here were the reduced ability
458 of IL-27R$^{-/-}$ HSCs post-infection to compete with WT HSCs, as well as the inability of these HSCs
459 to reconstitute upon secondary transfer, hallmarks of functional exhaustion (Singh et al., 2020).
460 These results infer that the ability of IL-27 to limit emergency myelopoiesis is also associated with
461 the ability of IL-27 to limit HSC exhaustion. Aberrant HSPC responses are associated with
462 conditions such as clonal hematopoiesis and aging, and there has been interest in the development
463 of strategies to target these HSPCs. Thus, selective targeting and depletion of "aged" HSPCs via
464 anti-CD150 treatments has been reported to restore balanced hematopoietic output and "youthful"

465 blood phenotypes (Ross et al., 2024). Whether IL-27 treatment can be used to preserve HSPCs, or
466 be blocked to enhance monocyte production, remains to be tested.

467 A common feature of certain models of innate training that affect hematopoiesis is that
468 cytokines, such as IFN-γ and IL-6, promote long term changes that polarize HSPCs toward
469 myeloid differentiation (Cheong et al., 2023; Kaufmann et al., 2018; Khan et al., 2020). Inherent
470 in this process is the idea that HSCs or downstream progeny would be sensitive to different
471 cytokines. The ability to survey the expression of cytokine receptors that influence hematopoiesis
472 emphasized that the shared cytokine receptor chains gp130 and IL-2Rγ are uniformly
473 expressed throughout hematopoietic development. In contrast, the alpha chain receptors for
474 individual cytokines (IL-6Rα, GM-CSFRα, IL-10R, IFNγRβ, IFNAR, IL-21R, TNFRI, and
475 TNFRII) displayed a much more restricted pattern of expression that correlated with key
476 features of the biology of individual cytokines. For example, the limited expression of the IL-
477 6 receptor on downstream progeny is consistent with reports of its high expression on MPPs
478 but not on HSCs (Mirantes et al., 2014; Reynaud et al., 2011). Nevertheless, that HSCs express
479 high levels of the IL-27R, which decreases with differentiation, emphasizes that these stem
480 cells are especially sensitive to the effects of IL-27. Whether IL-27 tempers some of the
481 processes associated with innate training or is itself associated with long-term epigenetic
482 changes is the subject of ongoing studies.

483 The use of murine models of toxoplasmosis have revealed many of the inhibitory
484 activities of IL-27, and the datasets presented here highlight the ability of IL-27 to influence
485 HSPCs to restrain monocyte/macrophage induction. There are also reports during other
486 infections and models that show IL-27 can regulate neutrophil and monocyte development
487 (Furusawa et al., 2016; Liu et al., 2014; Liu et al., 2021; Seita et al., 2008; Sun et al., 2017; Wirtz

488 et al., 2006). For example, during infection with an attenuated strain of *Plasmodium berghei,* IL-
489 27 was required for the induction of a neutrophil response, and *in vitro* IL-27 blunted the ability
490 of HSPCs to differentiate into the macrophage lineage (Furusawa et al., 2016). However, in less
491 inflammatory settings, such as tumor growth, the overexpression of IL-27 resulted in LSK
492 expansion and the induction of an M1 macrophage population (Zhu et al., 2023). Likewise, in a
493 model of angiotensin-mediated atherosclerosis, IL-27 was needed to overcome HSC quiescence
494 and increase differentiation and output of mature myeloid cells (Peshkova et al., 2019). While it
495 can be difficult to ascribe some of these effects to IL-27 acting directly on HSC, the contrasting
496 nature of these data sets suggest that the impact of IL-27 on HSPCs is context dependent. Indeed,
497 reports that TNFα can upregulate HSPC expression of the IL-27R (He et al., 2020) suggests that
498 IL-27 responsiveness can be regulated by the local environment. A better appreciation of these
499 environmental signals at homeostasis and during different types of inflammation, then, should help
500 to define these context-dependent activities of IL-27 on hematopoiesis.
501
502 **Acknowledgments and funding**
503 We would like to thank Dr. Nancy Speck for generously providing us with the Procr-cre
504 mouse line. Additionally, we thank Dr. Gordon Ruthel for his assistance and instruction in
505 capturing images of the mouse bone marrow. Schematic were created using BioRender (agreement
506 license BU27RCNPBH).
507 Funding for this work was provided by the NIH equipment grant (S10 OD032305-01A1),
508 NIH fellowship support (F31 AI 161962-03), and the Emmerson Foundation.
509
510

511 **Figure legends**

512 **Figure 1. IL-27 regulates monopoiesis during infection.** A) Schematic of infection and TAM
513 dosing strategy for Procr-Ai6 mice. B) Procr-Ai6 mice were infected and representative flow plots
514 of LTHSCs (Lin (CD3, NK1.1, B220, Ly6G)$^{-}$, Sca-1^{+}, CD117 (cKit)$^{+}$, CD135^{-}, CD48^{-}, CD150^{+})
515 from naïve (left) and infected (right) mice are shown. Proportions of zsGreen^{+} LTHSCs were then
516 quantified in both groups. C) Proportions of zsGreen^{+} monocytes (CD3^{-}, B220^{-}, CD11b^{+}, Ly6C^{+},
517 Ly6G^{-}) in the spleen and PECs of naïve and infected mice. D) Schematic of infection of WT and
518 IL-27p28$^{-/-}$ mice for E-F. E) Numbers of LTHSCs and granulocyte progenitors (GPs) (CD3^{-},
519 NK1.1^{-}, B220^{-}, CD117^{+}, CD34^{+}, CD16/32^{hi}, Ly6C^{+}, CD135^{-}, CD115^{-}) in the bone marrow of WT
520 and IL-27p28$^{-/-}$ infected mice throughout infection. F) Monocyte progenitors (MPs) (CD3^{-}, NK1.1^{-}
521 , B220^{-}, CD117^{+}, CD34^{+}, CD16/32^{hi}, Ly6C^{+}, CD135^{-}, CD115^{+}; orange box) in the bone marrow
522 of infected WT and IL-27p28$^{-/-}$ mice throughout infection. Representative flow plots are shown
523 (left) and quantified (right). Statistical significance was tested by one-way ANOVA with Sidak's
524 correction. *, **, and *** correspond to p-values $\leq$ 0.05, 0.01, and 0.001, respectively. N=3-5
525 mice/group and data shown are representative of 2-3 experiments.

526

527 **Supplemental Figure 1. IL-27 regulates monopoiesis during infection.** A) The proportion of
528 zsGreen^{+} monocyte dendritic cell progenitors (MDPs) (CD3^{-}, NK1.1^{-}, B220^{-}, CD117^{+}, CD34^{+},
529 CD16/32^{lo}, CD115^{+}), monocytes, and neutrophils (CD3^{-}, B220^{-}, CD11b^{+}, Ly6C^{+}, Ly6G^{+}) in the
530 BM of naïve and infected Procr-Ai6 mice. B) The proportion of zsGreen^{+} CCR2$^{hi/lo}$ CX3CR1$^{hi/lo}$
531 monocytes in the spleen and PECs in naïve and infected Procr-Ai6 mice. C) Number of MDPs in
532 WT and IL-27p28$^{-/-}$ mice in the bone marrow during infection. D) Numbers of monocytes in the
533 liver in WT and IL-27p28$^{-/-}$ throughout infection. E) WT and IL-27p28$^{-/-}$ mice were injected I.V.

534 with fluorescent anti-CD45 to label immune cells in the vasculature. Numbers of I.V. label^{-} and
535 CCR2^{hi}CX3CR1^{lo} monocytes in the liver were then quantified throughout infection. Statistical
536 significance was tested by one-way ANOVA with Sidak's correction. *, **, and *** correspond to
537 p-values $\leq$ 0.05, 0.01, and 0.001, respectively. N=3-5 mice/group and data shown are
538 representative of 2-3 experiments.
539
540 **Supplemental Figure 2. Gating strategy for flow cytometric analysis of cells in the bone**
541 **marrow and periphery.** Representative flow plots from the bone marrow (top) and spleen
542 (bottom) are shown indicating the gating strategy used to identify various cell populations. The
543 combination of surface markers used are listed in the tables (bottom) and are color coded to
544 correspond to both the developmental schematic pictured as well as the corresponding flow gate
545 on the representative plots.
546
547 **Figure 2. IL-27 regulates monopoiesis during infection in a cell intrinsic manner.** A) CD4-IL-
548 27R mice were infected and MPs (orange box) measured at 5 dpi in the BM. Representative flow
549 plots are shown (left) and quantified (right). B) Schematic of BM chimeras generated from WT
550 (CD45.1) and IL-27R$^{-/-}$ (CD45.1.2) bulk bone marrow that were then infected and used in C-D. C)
551 The proportion of LTHSCs (left) and MPs (right) from each respective donor lineage in the bone
552 marrow of both the single (left two bars) and mixed (right two bars) chimeras at 5 dpi. D)
553 Representative flow plots pre-gated on splenic monocytes (left plot) and then down-gated on
554 CCR2^{hi}CX3CR1^{lo} (right plot) monocytes at 5 dpi. WT derived monocytes are shown in the solid-
555 dark gray while IL-27R$^{-/-}$ derived cells are in the dashed-light gray. The proportion of each donor
556 lineage that contribute to mature CCR2^{hi}CX3CR1^{lo} splenic monocytes at 5 dpi were then

557 quantified (far right). Statistical significance was tested by either Welch's T-test (A) or one-way
558 ANOVA with Sidak's correction (C-D). *, **, and *** correspond to p-values ≤ 0.05, 0.01, and
559 0.001, respectively. N=3-5 mice/group and data shown are representative of 2-3 experiments.
560
561
562 **Supplemental Figure 3. IL-27 regulates monopoiesis during infection and post-irradiation in**
563 **a cell intrinsic manner.** A) IL-27Rα expression on $CD4^+$ ($CD19^-CD3^+CD8\alpha^-$) T cells, $CD8^+$
564 ($CD19^-CD3^+CD4^-$) T cells, and B cells ($CD19^+CD3^-$) in CD4-27R mice at 5 dpi. B) The proportion
565 of LTHSCs (left) and MPs (right) from each respective donor lineage in the bone marrow post-
566 reconstitution and pre-infection. C) The proportion of $CCR2^{hi}CX3CR1^{lo}$ monocytes from each
567 respective donor lineage in the spleen and liver post-reconstitution and pre-infection. Statistical
568 significance was tested by one-way ANOVA with Sidak's correction. *, **, and *** correspond to
569 p-values ≤ 0.05, 0.01, and 0.001, respectively. N=3-5 mice/group and data shown are
570 representative of 2 repeated experiments.
571
572 **Figure 3. IL-27p28 is produced in the BM during infection.** A) WT mice were infected, and the
573 bone marrow harvested throughout infection. BM was either washed with media or cultured for
574 24 hrs. and supernatant collected. Both the wash and supernatant were analyzed by ELISA for IL-
575 27p28. B) IL-27p28-GFP reporter mice were infected and their bone marrow analyzed by flow
576 cytometry throughout infection. A representative flow plot at 5 dpi of bulk marrow is shown (left)
577 and proportion of immune cell contribution to the GFP^+ population measured (right). C) Numbers
578 of IL-27p28-GFP^+ cells in the spleen, blood, and BM of infected mice were quantified throughout
579 infection (left). Proportions of GFP^+ $CD45^+$ cells were analyzed by cell type in the blood, spleen,

580 and PEC during infection (left). D) Femurs from infected Procr-tdTomato$^+$p28-GFP$^+$ mice were
581 harvested, sectioned, and imaged at 40x magnification. The total imaged femur is shown (top),
582 with zoomed in sections shown below for increased detail of cellular localization (bottom).
583 Numbers of Procr-tdTomato$^+$ and p28-GFP$^+$ cells were counted in eight randomly selected regions
584 throughout the marrow (see Supp. Fig. 4). GFP$^+$ cells were normalized to tdTomato$^+$ cells and the
585 eight counted regions classified as areas of hyper- or hypo-vascularization according to proximity
586 of the region to the labeled vasculature. This allowed quantification of the localization of cells
587 (bottom right).
588
589 **Supplemental Figure 4. IL-27p28 is produced in the bone marrow during infection.** A) IL-
590 27p28-GFP mice were infected, and the numbers of each CD45$^+$, immune cell type that expressed
591 GFP in the BM or periphery quantified throughout infection. B) Levels of IL-27p28-GFP
592 expression were measured in bulk monocytes (red) and dendritic cells (blue) in the bone marrow
593 (left) and spleen (right). C) Femurs from naïve IL-27p28-GFP mice were stained for Sca-1 and
594 imaged at 40x magnification. Zoomed in images are shown (right) of the indicated areas, with the
595 yellow arrows indicating positively stained, Sca-1$^+$ cells. D) The merged image shown in Fig. 3D
596 is separated by channel (GFP, tdTomato, and AF647, from top to bottom). Eight randomly selected
597 regions that were used for quantification of either GFP$^+$ or tdTomato$^+$ cells are shown (top), and
598 the quantification of cells in each region is shown next to the corresponding florescence channel
599 (right).
600
601 **Figure 4. Expression of the IL-27R subunits gp130 and IL-27Rα during hematopoietic**
602 **development.** A) Schematic ball-and-stick model of hierarchical hematopoietic development. Cell

603 type colors are maintained for reference in the following panels. B) Progenitors and progeny shown
604 in (A) were analyzed in WT and infected mice (at 5 dpi) by flow cytometry for the gp130 receptor.
605 10,000 live cells were concatenated from n=3 mice, and representative flow plots are shown. C)
606 Cells in (B) were analyzed for expression of the IL-27Rα. D) Bulk bone marrow was isolated from
607 IRGM1-dsRed reporter mice. 22 x 10^6 cells were plated per condition and stimulated with 20 ng/ml
608 of IL-27 for 0, 6, or 48 hours and RFP expression measured by flow cytometry.
609
610 **Supplemental Figure 5. IL-27Rα transcript expression during hematopoiesis and differential**
611 **sensitivity of LTHSC and CMP to IL-27.** A) Expression levels of *IL27RA* are shown from the
612 Haemosphere RNA-seq data set and online tool as well as the Blood Spot data set and visualizer
613 (B). C) Representative flow plots of IRGM1-RFP expression in LTHSCs and CMPs 48 hrs. post-
614 stimulation with IL-27.
615
616 **Figure 5. Developmental expression of hematopoietic cytokine receptors.** A) Expression of
617 CD132 (IL-2Rγ) and B) CD131 (GM-CSF/IL-3/IL-5Rβ) was analyzed by flow cytometry on
618 progenitors and progeny in the BM of naïve and 5 dpi mice as in Fig. 4. C) Expression of IL-6Rα
619 and D) GM-CSFRα were measured as in (A).
620
621 **Supplemental Figure 6. Developmental expression of additional cytokine receptors.** Indicated
622 cytokine receptors were analyzed in naive and infected mice as described in Fig. 4-5.
623
624 **Figure 6. IL-27 limits infection induced HSPC polarization.** WT and IL-27R$^{-/-}$ mice were
625 infected for 5 days, LTHSCs sorted, and cultured in MethoCult for 10-12 days before being

626 analyzed by flow cytometry. A) 10,000 live cells from n=3-4 mice/ group (WT (naïve+5 dpi) and
627 IL-27R$^{-/-}$ (5 dpi)) were concatenated and dimensionally reduced via UMAP. B) Numbers of cells
628 in each cluster from (A) were measured. C) X-shift analysis was used to identify the expression
629 level of each marker used in the clustering performed in (A). 5 of the dominant clusters from (B)
630 are shown. D) Clusters 1, 10, and 11, all involved in monocyte development, are highlighted. E)
631 Contribution of Clusters 1, 10, and 11 to each genotype are shown (left) and quantified (right). F)
632 Bone marrow chimeras were generated from infected WT and IL-27R$^{-/-}$ mice (left). The
633 contribution of donor cells to mature monocytes was then measured at 14 weeks post-transplant
634 (right). Statistical significance was tested by one-way ANOVA with Sidak's correction. *, ***, and
635 **** correspond to p-values ≤ 0.05, 0.001, and 0.0001, respectively. N=3-5 mice/group and data
636 shown are representative of 2-3 repeated experiments.
637
638 **Supplemental Figure 7. Gating strategy for sorting of LTHSCs used in monocyte**
639 **differentiation.** LTHSCs were sorted from WT naïve, WT 5 dpi, and IL-27R$^{-/-}$ 5 dpi mice. The
640 gating strategy is shown as well as the purity of sorted samples (last panel).
641
642 **Supplemental Figure 8. Development and validation of an unbiased flow cytometry approach**
643 **for the analysis of MethoCult colonies.** WT and IL-27R$^{-/-}$ mice were infected, LTHSCs sorted
644 and cultured in MethoCult for either 5 or 10 days. A) Colony phenotypes were analyzed by
645 microscopy and counted by eye. B) Colonies were collected at either 5 or 10 days post-culture
646 (dpc) and analyzed by flow cytometry. 500 live cells from n=3-4 mice/ group were concatenated
647 and dimensionally reduced via UMAP. UMAP plots are shown, and Ki67 expression is overlayed.
648 C) X-shift analysis was used to identify the expression level of each marker used in the clustering

649 performed in (B). D) Numbers of cells in each cluster from (B) were measured. E) Contribution of
650 each genotype to each cluster was quantified. Statistical significance was tested by one-way
651 ANOVA with Sidak's correction. *, ***, and **** correspond to p-values ≤ 0.05, 0.001, and
652 0.0001, respectively. N=3-4 mice/group and data shown are from 1 of 3 experiments.
653
654 **Figure 7. Testing the impact of IL-27 on functionality and fitness of HSPCs during infection.**
655 A) WT and IL-27R$^{-/-}$ were infected, treated with 5 mg BRDU, and kept on 1mg/ml BRDU in the
656 drinking water throughout infection. Incorporation of BRDU was then measured in Lin^{-}Sca-
657 1^{+}cKit^{+} (LSK) progenitor cells in comparison to Ki67 at 5 dpi. Representative flow plots are shown
658 (left) and the proportion of BRDU^{+}Ki67^{+} cells quantified (right). B) Schematic for the generation
659 of BM chimeras from infected mice used in (C). C) Numbers of LTHSCs from recipients receiving
660 donor marrow from either uninfected or infected mice were measured based on genotype. D)
661 Secondary transplant chimeras from mice that originally received naïve or infected marrow where
662 generated as shown (left). Survival of recipients was then assessed (right).
663
664 **Supplemental Figure 9. Testing HSPC survival and fitness.** A) LTHSCs from WT and IL-27R^{-}
665 $^{/-}$ BM at 5 dpi was stained for Annexin V (AV) expression and free-amine staining viability dye
666 (LD). This allowed the measurement of apoptotic (AV^{+}LD^{-}), late apoptotic (AV^{+}LD^{+}), and necrotic
667 (AV^{-}LD^{+}) cells. The proportion of LTHSCs in each of these stages was quantified. B) Monocyte
668 genotype was analyzed at 9 weeks post-transplant (wpt) from either naïve WT (CD45.1) or IL-
669 27R$^{-/-}$ (CD45.1.2) donors (top) or from infected donors (bottom), including a 1:1 mix of infected
670 WT and IL-27R$^{-/-}$ donors. Statistical significance was tested by Welch's t-test.
671

672

673 **References**

674 Aldridge, D.L., D. Moodley, J. Park, A.T. Phan, M. Rausch, K.F. White, Y. Ren, K. Golin, E. Radaelli, R.
675 Kedl, P.M. Holland, J. Hill, and C.A. Hunter. 2024. Endogenous IL-27 during toxoplasmosis
676 limits early monocyte responses and their inflammatory activation by pathological T cells.
677 *mBio* 15:e0008324.
678 Askenase, M.H., S.J. Han, A.L. Byrd, D. Morais da Fonseca, N. Bouladoux, C. Wilhelm, J.E. Konkel,
679 T.W. Hand, N. Lacerda-Queiroz, X.Z. Su, G. Trinchieri, J.R. Grainger, and Y. Belkaid. 2015.
680 Bone-Marrow-Resident NK Cells Prime Monocytes for Regulatory Function during
681 Infection. *Immunity* 42:1130-1142.
682 Au - Amend, S.R., K.C. Au - Valkenburg, and K.J. Au - Pienta. 2016. Murine Hind Limb Long Bone
683 Dissection and Bone Marrow Isolation. *JoVE* e53936.
684 Bagger, F.O., D. Sasivarevic, S.H. Sohi, L.G. Laursen, S. Pundhir, C.K. Sønderby, O. Winther, N. Rapin,
685 and B.T. Porse. 2015. BloodSpot: a database of gene expression profiles and transcriptional
686 programs for healthy and malignant haematopoiesis. *Nucleic Acids Research* 44:D917-
687 D924.
688 Baldridge, M.T., K.Y. King, N.C. Boles, D.C. Weksberg, and M.A. Goodell. 2010. Quiescent
689 haematopoietic stem cells are activated by IFN-gamma in response to chronic infection.
690 *Nature* 465:793-797.
691 Baldridge, M.T., K.Y. King, and M.A. Goodell. 2011. Inflammatory signals regulate hematopoietic
692 stem cells. *Trends Immunol* 32:57-65.
693 Caiado, F., E.M. Pietras, and M.G. Manz. 2021. Inflammation as a regulator of hematopoietic stem
694 cell function in disease, aging, and clonal selection. *Journal of Experimental Medicine* 218:
695 Chambers, S.M., N.C. Boles, K.Y. Lin, M.P. Tierney, T.V. Bowman, S.B. Bradfute, A.J. Chen, A.A.
696 Merchant, O. Sirin, D.C. Weksberg, M.G. Merchant, C.J. Fisk, C.A. Shaw, and M.A. Goodell.
697 2007. Hematopoietic fingerprints: an expression database of stem cells and their progeny.
698 *Cell Stem Cell* 1:578-591.
699 Chapple, R.H., Y.J. Tseng, T. Hu, A. Kitano, M. Takeichi, K.A. Hoegenauer, and D. Nakada. 2018.
700 Lineage tracing of murine adult hematopoietic stem cells reveals active contribution to
701 steady-state hematopoiesis. *Blood Adv* 2:1220-1228.
702 Cheong, J.G., A. Ravishankar, S. Sharma, C.N. Parkhurst, S.A. Grassmann, C.K. Wingert, P. Laurent,
703 S. Ma, L. Paddock, I.C. Miranda, E.O. Karakaslar, D. Nehar-Belaid, A. Thibodeau, M.J. Bale,
704 V.K. Kartha, J.K. Yee, M.Y. Mays, C. Jiang, A.W. Daman, A. Martinez de Paz, D. Ahimovic, V.
705 Ramos, A. Lercher, E. Nielsen, S. Alvarez-Mulett, L. Zheng, A. Earl, A. Yallowitz, L. Robbins,
706 E. LaFond, K.L. Weidman, S. Racine-Brzostek, H.S. Yang, D.R. Price, L. Leyre, A.F. Rendeiro,
707 H. Ravichandran, J. Kim, A.C. Borczuk, C.M. Rice, R.B. Jones, E.J. Schenck, R.J. Kaner, A.
708 Chadburn, Z. Zhao, V. Pascual, O. Elemento, R.E. Schwartz, J.D. Buenrostro, R.E. Niec, F.J.
709 Barrat, L. Lief, J.C. Sun, D. Ucar, and S.Z. Josefowicz. 2023. Epigenetic memory of
710 coronavirus infection in innate immune cells and their progenitors. *Cell* 186:3882-
711 3902.e3824.
712 Choi, J., T.M. Baldwin, M. Wong, J.E. Bolden, K.A. Fairfax, E.C. Lucas, R. Cole, C. Biben, C. Morgan,
713 K.A. Ramsay, A.P. Ng, M. Kauppi, L.M. Corcoran, W. Shi, N. Wilson, M.J. Wilson, W.S.

714 Alexander, D.J. Hilton, and C.A. de Graaf. 2018. Haemopedia RNA-seq: a database of gene
715 expression during haematopoiesis in mice and humans. *Nucleic Acids Research* 47:D780-
716 D785.
717 Christian, D.A., A.A. Koshy, M.A. Reuter, M.R. Betts, J.C. Boothroyd, and C.A. Hunter. 2014. Use of
718 transgenic parasites and host reporters to dissect events that promote interleukin-12
719 production during toxoplasmosis. *Infect Immun* 82:4056-4067.
720 Collins, A., C.A. Mitchell, and E. Passegué. 2021. Inflammatory signaling regulates hematopoietic
721 stem and progenitor cell development and homeostasis. *Journal of Experimental Medicine*
722 218:
723 Collins, A., J.W. Swann, M.A. Proven, C.M. Patel, C.A. Mitchell, M. Kasbekar, P.V. Dellorusso, and E.
724 Passegué. 2024. Maternal inflammation regulates fetal emergency myelopoiesis. *Cell*
725 187:1402-1421.e1421.
726 Detavernier, A., A. Azouz, H. Shehade, M. Splittgerber, L. Van Maele, M. Nguyen, S. Thomas, Y.
727 Achouri, D. Svec, E. Calonne, F. Fuks, G. Oldenhove, and S. Goriely. 2019. Monocytes
728 undergo multi-step differentiation in mice during oral infection by Toxoplasma gondii.
729 *Commun Biol* 2:472.
730 Di Tullio, A., T.P. Vu Manh, A. Schubert, G. Castellano, R. Månsson, and T. Graf. 2011.
731 CCAAT/enhancer binding protein alpha (C/EBP(alpha))-induced transdifferentiation of
732 pre-B cells into macrophages involves no overt retrodifferentiation. *Proc Natl Acad Sci U S*
733 *A* 108:17016-17021.
734 Do, J., D. Kim, S. Kim, A. Valentin-Torres, N. Dvorina, E. Jang, V. Nagarajavel, T.M. DeSilva, X. Li,
735 A.H. Ting, D.A.A. Vignali, S.A. Stohlman, W.M. Baldwin, 3rd, and B. Min. 2017. Treg-specific
736 IL-27Rα deletion uncovers a key role for IL-27 in Treg function to control autoimmunity.
737 *Proc Natl Acad Sci U S A* 114:10190-10195.
738 Dunay, I.R., R.A. Damatta, B. Fux, R. Presti, S. Greco, M. Colonna, and L.D. Sibley. 2008. Gr1(+)
739 inflammatory monocytes are required for mucosal resistance to the pathogen Toxoplasma
740 gondii. *Immunity* 29:306-317.
741 Eliasson, P., and J.I. Jönsson. 2010. The hematopoietic stem cell niche: low in oxygen but a nice
742 place to be. *J Cell Physiol* 222:17-22.
743 Feng, C.G., D.C. Weksberg, G.A. Taylor, A. Sher, and M.A. Goodell. 2008. The p47 GTPase Lrg-47
744 (Irgm1) Links Host Defense and Hematopoietic Stem Cell Proliferation. *Cell Stem Cell* 2:83-
745 89.
746 Findlay, E.G., R. Greig, J.S. Stumhofer, J.C. Hafalla, J.B. de Souza, C.J. Saris, C.A. Hunter, E.M. Riley,
747 and K.N. Couper. 2010. Essential role for IL-27 receptor signaling in prevention of Th1-
748 mediated immunopathology during malaria infection. *J Immunol* 185:2482-2492.
749 Furusawa, J., I. Mizoguchi, Y. Chiba, M. Hisada, F. Kobayashi, H. Yoshida, S. Nakae, A. Tsuchida, T.
750 Matsumoto, H. Ema, J. Mizuguchi, and T. Yoshimoto. 2016. Promotion of Expansion and
751 Differentiation of Hematopoietic Stem Cells by Interleukin-27 into Myeloid Progenitors to
752 Control Infection in Emergency Myelopoiesis. *PLoS Pathog* 12:e1005507.
753 Gur-Cohen, S., T. Itkin, S. Chakrabarty, C. Graf, O. Kollet, A. Ludin, K. Golan, A. Kalinkovich, G.
754 Ledergor, E. Wong, E. Niemeyer, Z. Porat, A. Erez, I. Sagi, C.T. Esmon, W. Ruf, and T. Lapidot.
755 2015. PAR1 signaling regulates the retention and recruitment of EPCR-expressing bone
756 marrow hematopoietic stem cells. *Nat Med* 21:1307-1317.

757 Hall, A.O., D.P. Beiting, C. Tato, B. John, G. Oldenhove, C.G. Lombana, G.H. Pritchard, J.S. Silver, N.
758 Bouladoux, J.S. Stumhofer, T.H. Harris, J. Grainger, E.D. Wojno, S. Wagage, D.S. Roos, P.
759 Scott, L.A. Turka, S. Cherry, S.L. Reiner, D. Cua, Y. Belkaid, M.M. Elloso, and C.A. Hunter.
760 2012. The cytokines interleukin 27 and interferon-γ promote distinct Treg cell populations
761 required to limit infection-induced pathology. *Immunity* 37:511-523.
762 Hamano, S., K. Himeno, Y. Miyazaki, K. Ishii, A. Yamanaka, A. Takeda, M. Zhang, H. Hisaeda, T.W.
763 Mak, A. Yoshimura, and H. Yoshida. 2003. WSX-1 Is Required for Resistance to
764 Trypanosoma cruzi Infection by Regulation of Proinflammatory Cytokine Production.
765 *Immunity* 19:657-667.
766 He, H., P. Xu, X. Zhang, M. Liao, Q. Dong, T. Cong, B. Tang, X. Yang, M. Ye, Y. Chang, W. Liu, X. Wang,
767 Z. Ju, and J. Wang. 2020. Aging-induced IL27Ra signaling impairs hematopoietic stem cells.
768 *Blood* 136:183-198.
769 Ibneeva, L., S.P. Singh, A. Sinha, S.E. Eski, R. Wehner, L. Rupp, I. Kovtun, J.A. Pérez-Valencia, A.
770 Gerbaulet, S. Reinhardt, M. Wobus, M. von Bonin, J. Sancho, F. Lund, A. Dahl, M. Schmitz,
771 M. Bornhäuser, T. Chavakis, B. Wielockx, and T. Grinenko. 2024. CD38 promotes
772 hematopoietic stem cell dormancy. *PLoS Biol* 22:e3002517.
773 Im, K., S. Mareninov, M.F.P. Diaz, and W.H. Yong. 2019. An Introduction to Performing
774 Immunofluorescence Staining. *Methods Mol Biol* 1897:299-311.
775 Iwasaki, H., F. Arai, Y. Kubota, M. Dahl, and T. Suda. 2010. Endothelial protein C receptor-
776 expressing hematopoietic stem cells reside in the perisinusoidal niche in fetal liver. *Blood*
777 116:544-553.
778 John, B., T.H. Harris, E.D. Tait, E.H. Wilson, B. Gregg, L.G. Ng, P. Mrass, D.S. Roos, F. Dzierszinski,
779 W. Weninger, and C.A. Hunter. 2009. Dynamic Imaging of CD8(+) T cells and dendritic cells
780 during infection with Toxoplasma gondii. *PLoS Pathog* 5:e1000505.
781 Kaufmann, E., J. Sanz, J.L. Dunn, N. Khan, L.E. Mendonça, A. Pacis, F. Tzelepis, E. Pernet, A.
782 Dumaine, J.C. Grenier, F. Mailhot-Léonard, E. Ahmed, J. Belle, R. Besla, B. Mazer, I.L. King,
783 A. Nijnik, C.S. Robbins, L.B. Barreiro, and M. Divangahi. 2018. BCG Educates Hematopoietic
784 Stem Cells to Generate Protective Innate Immunity against Tuberculosis. *Cell* 172:176-
785 190.e119.
786 Khan, N., J. Downey, J. Sanz, E. Kaufmann, B. Blankenhaus, A. Pacis, E. Pernet, E. Ahmed, S.
787 Cardoso, A. Nijnik, B. Mazer, C. Sassetti, M.A. Behr, M.P. Soares, L.B. Barreiro, and M.
788 Divangahi. 2020. M. tuberculosis Reprograms Hematopoietic Stem Cells to Limit
789 Myelopoiesis and Impair Trained Immunity. *Cell* 183:752-770.e722.
790 Kilgore, A.M., S. Welsh, E.E. Cheney, A. Chitrakar, T.J. Blain, B.J. Kedl, C.A. Hunter, N.D. Pennock,
791 and R.M. Kedl. 2018. IL-27p28 Production by XCR1(+) Dendritic Cells and Monocytes
792 Effectively Predicts Adjuvant-Elicited CD8(+) T Cell Responses. *Immunohorizons* 2:1-11.
793 Kimura, D., M. Miyakoda, K. Kimura, K. Honma, H. Hara, H. Yoshida, and K. Yui. 2016. Interleukin-
794 27-Producing CD4(+) T Cells Regulate Protective Immunity during Malaria Parasite
795 Infection. *Immunity* 44:672-682.
796 King, K.Y., M.T. Baldridge, D.C. Weksberg, S.M. Chambers, G.L. Lukov, S. Wu, N.C. Boles, S.Y. Jung,
797 J. Qin, D. Liu, Z. Songyang, N.T. Eissa, G.A. Taylor, and M.A. Goodell. 2011. Irgm1 protects
798 hematopoietic stem cells by negative regulation of IFN signaling. *Blood* 118:1525-1533.
799 Lin, C.-H., C.-J. Wu, S. Cho, R. Patkar, W.J. Huth, L.-L. Lin, M.-C. Chen, E. Israelsson, J. Betts, M.
800 Niedzielska, S.A. Patel, H.G. Duong, R.R. Gerner, C.-Y. Hsu, M. Catley, R.A. Maciewicz, H.

801 Chu, M. Raffatellu, J.T. Chang, and L.-F. Lu. 2023. Selective IL-27 production by intestinal
802 regulatory T cells permits gut-specific regulation of TH17 cell immunity. *Nature*
803 *Immunology* 24:2108-2120.
804 Link, D.C. 2000. Mechanisms of granulocyte colony-stimulating factor-induced hematopoietic
805 progenitor-cell mobilization. *Semin Hematol* 37:25-32.
806 Liu, F.D.M., E.E. Kenngott, M.F. Schröter, A. Kühl, S. Jennrich, R. Watzlawick, U. Hoffmann, T. Wolff,
807 S. Norley, A. Scheffold, J.S. Stumhofer, C.J.M. Saris, J.M. Schwab, C.A. Hunter, G.F. Debes,
808 and A. Hamann. 2014. Timed Action of IL-27 Protects from Immunopathology while
809 Preserving Defense in Influenza. *PLOS Pathogens* 10:e1004110.
810 Liu, G., O. Abas, Y. Fu, Y. Chen, A.B. Strickland, D. Sun, and M. Shi. 2021. IL-27 Negatively Regulates
811 Tip-DC Development during Infection. *mBio* 12:
812 Liu, Y., Y. Chen, X. Deng, and J. Zhou. 2020. ATF3 Prevents Stress-Induced Hematopoietic Stem Cell
813 Exhaustion. *Front Cell Dev Biol* 8:585771.
814 Ma, Z., J. Xu, L. Wu, J. Wang, Q. Lin, F.A. Chowdhury, M.H.H. Mazumder, G. Hu, X. Li, and W. Du.
815 2020. Hes1 deficiency causes hematopoietic stem cell exhaustion. *Stem Cells* 38:756-768.
816 MacNamara, K.C., M. Jones, O. Martin, and G.M. Winslow. 2011a. Transient activation of
817 hematopoietic stem and progenitor cells by IFNγ during acute bacterial infection. *PLoS*
818 *One* 6:e28669.
819 MacNamara, K.C., K. Oduro, O. Martin, D.D. Jones, M. McLaughlin, K. Choi, D.L. Borjesson, and
820 G.M. Winslow. 2011b. Infection-induced myelopoiesis during intracellular bacterial
821 infection is critically dependent upon IFN-γ signaling. *J Immunol* 186:1032-1043.
822 Maeda, K., Y. Baba, Y. Nagai, K. Miyazaki, A. Malykhin, K. Nakamura, P.W. Kincade, N. Sakaguchi,
823 and K.M. Coggeshall. 2005. IL-6 blocks a discrete early step in lymphopoiesis. *Blood*
824 106:879-885.
825 Matatall, K.A., C.C. Shen, G.A. Challen, and K.Y. King. 2014. Type II interferon promotes
826 differentiation of myeloid-biased hematopoietic stem cells. *Stem Cells* 32:3023-3030.
827 McCabe, A., Y. Zhang, V. Thai, M. Jones, M.B. Jordan, and K.C. MacNamara. 2015. Macrophage-
828 Lineage Cells Negatively Regulate the Hematopoietic Stem Cell Pool in Response to
829 Interferon Gamma at Steady State and During Infection. *Stem Cells* 33:2294-2305.
830 Miner, X., Z. Shanshan, D. Fang, Z. Qingyun, W. Jinhong, W. Chenchen, Z. Caiying, Z. Sen, L.
831 Bingqing, W. Peng, and E. Hideo. 2021. Granulocyte colony-stimulating factor directly acts
832 on mouse lymphoid-biased but not myeloid-biased hematopoietic stem cells.
833 *Haematologica* 106:1647-1658.
834 Mirantes, C., E. Passegué, and E.M. Pietras. 2014. Pro-inflammatory cytokines: emerging players
835 regulating HSC function in normal and diseased hematopoiesis. *Exp Cell Res* 329:248-254.
836 Morales-Mantilla, D.E., B. Kain, D. Le, A.R. Flores, S. Paust, and K.Y. King. 2022. Hematopoietic
837 stem and progenitor cells improve survival from sepsis by boosting immunomodulatory
838 cells. *eLife* 11:e74561.
839 Ochando, J., W.J.M. Mulder, J.C. Madsen, M.G. Netea, and R. Duivenvoorden. 2023. Trained
840 immunity — basic concepts and contributions to immunopathology. *Nature Reviews*
841 *Nephrology* 19:23-37.
842 Pardy, R.D., K.A. Walzer, B.A. Wallbank, J.H. Byerly, K.M. O'Dea, I.S. Cohn, B.E. Haskins, J.L.
843 Roncaioli, E.J. Smith, G.Y. Buenconsejo, B. Striepen, and C.A. Hunter. 2024. Analysis of

intestinal epithelial cell responses to Cryptosporidium highlights the temporal effects of IFN-γ on parasite restriction. *PLOS Pathogens* 20:e1011820.

Parmar, K., P. Mauch, J.A. Vergilio, R. Sackstein, and J.D. Down. 2007. Distribution of hematopoietic stem cells in the bone marrow according to regional hypoxia. *Proc Natl Acad Sci U S A* 104:5431-5436.

Peshkova, I.O., T. Aghayev, A.R. Fatkhullina, P. Makhov, E.K. Titerina, S. Eguchi, Y.F. Tan, A.V. Kossenkov, M.V. Khoreva, L.V. Gankovskaya, S.M. Sykes, and E.K. Koltsova. 2019. IL-27 receptor-regulated stress myelopoiesis drives abdominal aortic aneurysm development. *Nature Communications* 10:5046.

Pflanz, S., L. Hibbert, J. Mattson, R. Rosales, E. Vaisberg, J.F. Bazan, J.H. Phillips, T.K. McClanahan, R. de Waal Malefyt, and R.A. Kastelein. 2004. WSX-1 and Glycoprotein 130 Constitute a Signal-Transducing Receptor for IL-27. *The Journal of Immunology* 172:2225-2231.

Pflanz, S., J.C. Timans, J. Cheung, R. Rosales, H. Kanzler, J. Gilbert, L. Hibbert, T. Churakova, M. Travis, E. Vaisberg, W.M. Blumenschein, J.D. Mattson, J.L. Wagner, W. To, S. Zurawski, T.K. McClanahan, D.M. Gorman, J.F. Bazan, R. de Waal Malefyt, D. Rennick, and R.A. Kastelein. 2002. IL-27, a Heterodimeric Cytokine Composed of EBI3 and p28 Protein, Induces Proliferation of Naive CD4+ T Cells. *Immunity* 16:779-790.

Pietras, E.M., R. Lakshminarasimhan, J.M. Techner, S. Fong, J. Flach, M. Binnewies, and E. Passegué. 2014. Re-entry into quiescence protects hematopoietic stem cells from the killing effect of chronic exposure to type I interferons. *J Exp Med* 211:245-262.

Revuelta, M., and A. Matheu. 2017. Autophagy in stem cell aging. *Aging Cell* 16:912-915.

Reynaud, D., E. Pietras, K. Barry-Holson, A. Mir, M. Binnewies, M. Jeanne, O. Sala-Torra, J.P. Radich, and E. Passegué. 2011. IL-6 controls leukemic multipotent progenitor cell fate and contributes to chronic myelogenous leukemia development. *Cancer Cell* 20:661-673.

Ross, J.B., L.M. Myers, J.J. Noh, M.M. Collins, A.B. Carmody, R.J. Messer, E. Dhuey, K.J. Hasenkrug, and I.L. Weissman. 2024. Depleting myeloid-biased haematopoietic stem cells rejuvenates aged immunity. *Nature* 628:162-170.

Samusik, N., Z. Good, M.H. Spitzer, K.L. Davis, and G.P. Nolan. 2016. Automated mapping of phenotype space with single-cell data. *Nat Methods* 13:493-496.

Säwen, P., M. Eldeeb, E. Erlandsson, T.A. Kristiansen, C. Laterza, Z. Kokaia, G. Karlsson, J. Yuan, S. Soneji, P.K. Mandal, D.J. Rossi, and D. Bryder. 2018. Murine HSCs contribute actively to native hematopoiesis but with reduced differentiation capacity upon aging. *eLife* 7:e41258.

Schindelin, J., I. Arganda-Carreras, E. Frise, V. Kaynig, M. Longair, T. Pietzsch, S. Preibisch, C. Rueden, S. Saalfeld, B. Schmid, J.-Y. Tinevez, D.J. White, V. Hartenstein, K. Eliceiri, P. Tomancak, and A. Cardona. 2012. Fiji: an open-source platform for biological-image analysis. *Nature Methods* 9:676-682.

Seita, J., M. Asakawa, J. Ooehara, S. Takayanagi, Y. Morita, N. Watanabe, K. Fujita, M. Kudo, J. Mizuguchi, H. Ema, H. Nakauchi, and T. Yoshimoto. 2008. Interleukin-27 directly induces differentiation in hematopoietic stem cells. *Blood* 111:1903-1912.

Seyfried, A.N., J.M. Maloney, and K.C. MacNamara. 2020. Macrophages Orchestrate Hematopoietic Programs and Regulate HSC Function During Inflammatory Stress. *Front Immunol* 11:1499.

887 Siminovitch, L., J.E. Till, and E.A. McCulloch. 1964. Decline in colony-forming ability of marrow
888 cells subjected to serial transplantation into irradiated mice. *Journal of Cellular and*
889 *Comparative Physiology* 64:23-31.
890 Singh, S., B. Jakubison, and J.R. Keller. 2020. Protection of hematopoietic stem cells from stress-
891 induced exhaustion and aging. *Curr Opin Hematol* 27:225-231.
892 Singh, S.K., S. Singh, S. Gadomski, L. Sun, A. Pfannenstein, V. Magidson, X. Chen, S. Kozlov, L.
893 Tessarollo, K.D. Klarmann, and J.R. Keller. 2018. Id1 Ablation Protects
894 Hematopoietic Stem Cells from Stress-Induced Exhaustion and Aging. *Cell Stem Cell*
895 23:252-265.e258.
896 Stifter, S.A., N. Bhattacharyya, A.J. Sawyer, T.A. Cootes, J. Stambas, S.E. Doyle, L. Feigenbaum, W.E.
897 Paul, W.J. Britton, A. Sher, and C.G. Feng. 2019. Visualizing the Selectivity and Dynamics of
898 Interferon Signaling In Vivo. *Cell Rep* 29:3539-3550.e3534.
899 Sun, D., M. Zhang, and M. Shi. 2017. IL-27 limits neutrophil mediated pathology during pulmonary
900 infection with Cryptococcus neoformans. *The Journal of Immunology* 198:123.128-
901 123.128.
902 Villarino, A., L. Hibbert, L. Lieberman, E. Wilson, T. Mak, H. Yoshida, R.A. Kastelein, C. Saris, and
903 C.A. Hunter. 2003. The IL-27R (WSX-1) is required to suppress T cell hyperactivity during
904 infection. *Immunity* 19:645-655.
905 Weissman, I.L. 2000. Stem Cells: Units of Development, Units of Regeneration, and Units in
906 Evolution. *Cell* 100:157-168.
907 Wirtz , S., I. Tubbe , P.R. Galle , H.J. Schild , M. Birkenbach , R.S. Blumberg , and M.F. Neurath 2006.
908 Protection from lethal septic peritonitis by neutralizing the biological function of
909 interleukin 27. *Journal of Experimental Medicine* 203:1875-1881.
910 Zhao, H.G., and M. Deininger. 2023. Always stressed but never exhausted: how stem cells in
911 myeloid neoplasms avoid extinction in inflammatory conditions. *Blood* 141:2797-2812.
912 Zhu, J., J. Yu, A. Hu, J.Q. Liu, X. Pan, G. Xin, W.E. Carson, Z. Li, Y. Yang, and X.F. Bai. 2023. IL-27 Gene
913 Therapy Induces Stat3-Mediated Expansion of CD11b+Gr1+ Myeloid Cells and Promotes
914 Accumulation of M1 Macrophages in the Tumor Microenvironment. *J Immunol* 211:895-
915 902.
916

Figure 1

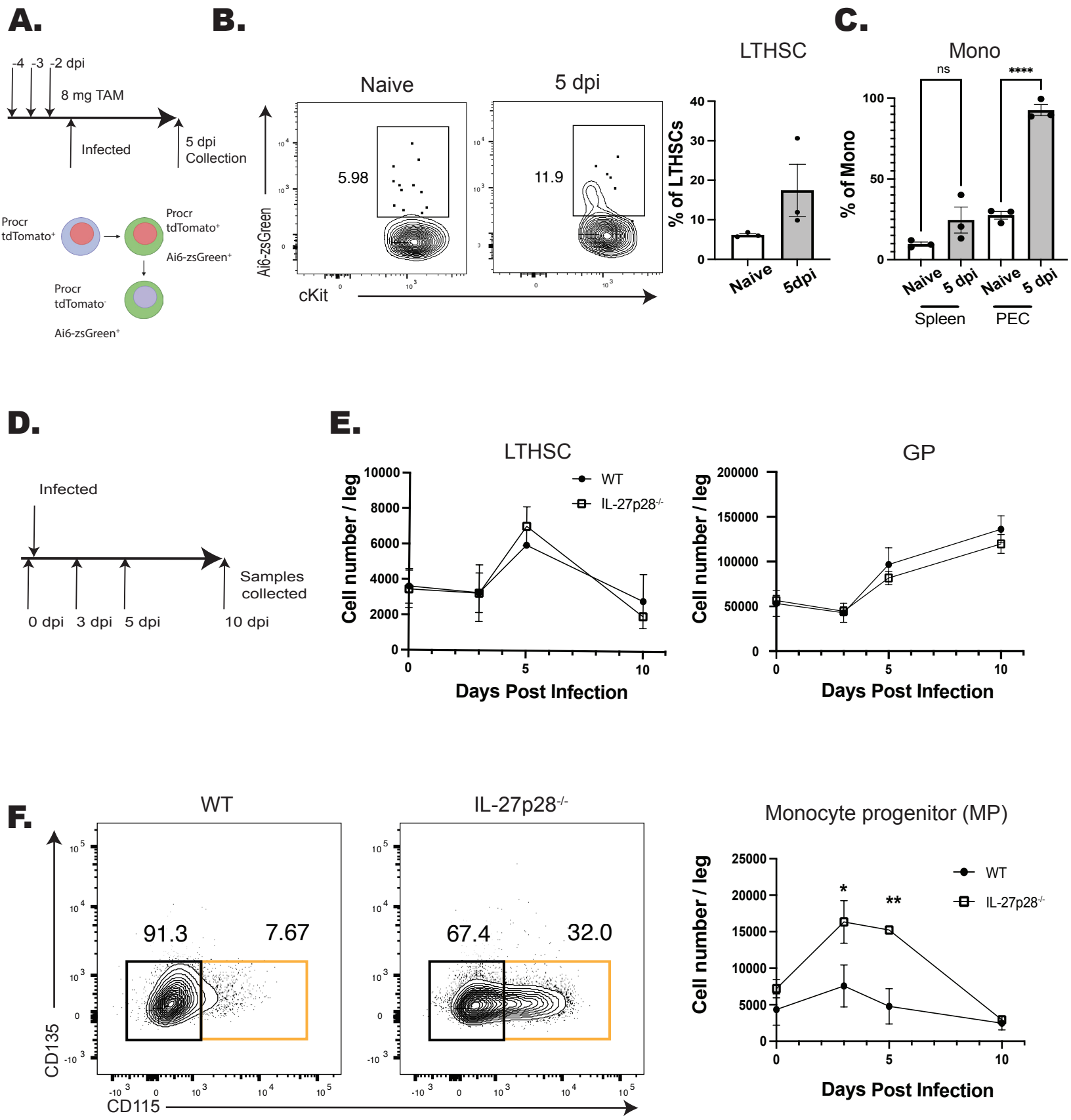
A.
-4 -3 -2 dpi
8 mg TAM
Infected
5 dpi Collection
Procr tdTomato+
Procr tdTomato+
Ai6-zsGreen+
Procr tdTomato-
Ai6-zsGreen+
B.
Naive
5 dpi
5.98
11.9
Ai6-zsGreen
cKit
LTHSC
% of LTHSCs
Naive
5dpi
C.
Mono
ns
****
% of Mono
Naive
5 dpi
Naive
5 dpi
Spleen
PEC
D.
Infected
Samples collected
0 dpi
3 dpi
5 dpi
10 dpi
E.
LTHSC
GP
WT
IL-27p28-/-
Cell number / leg
Days Post Infection
F.
WT
IL-27p28-/-
91.3
7.67
67.4
32.0
CD135
CD115
Monocyte progenitor (MP)
Cell number / leg
Days Post Infection
WT
IL-27p28-/-
*
**

Supplemental Figure 1

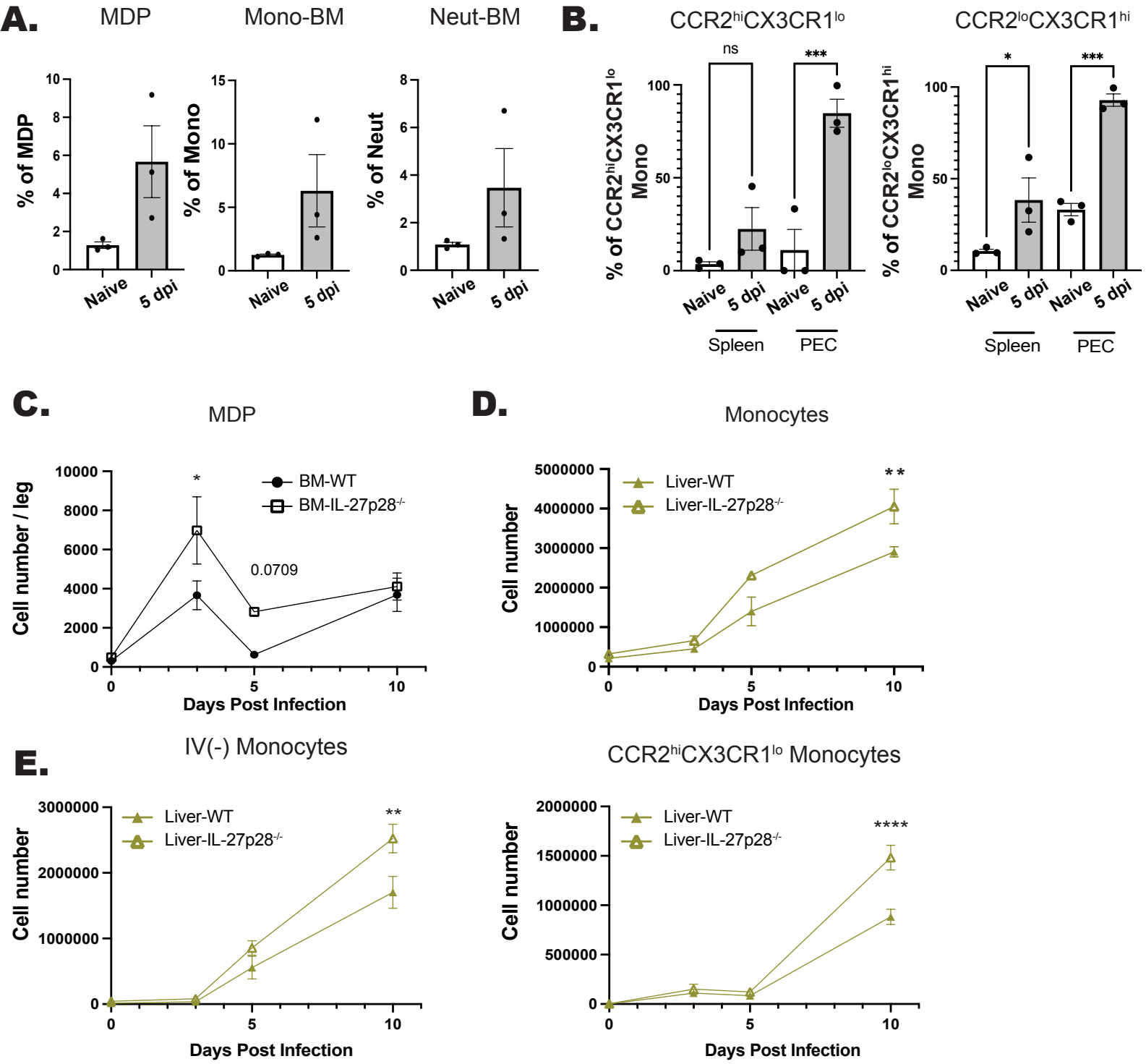

Supplemental Figure 2

Bone marrow gating strategy

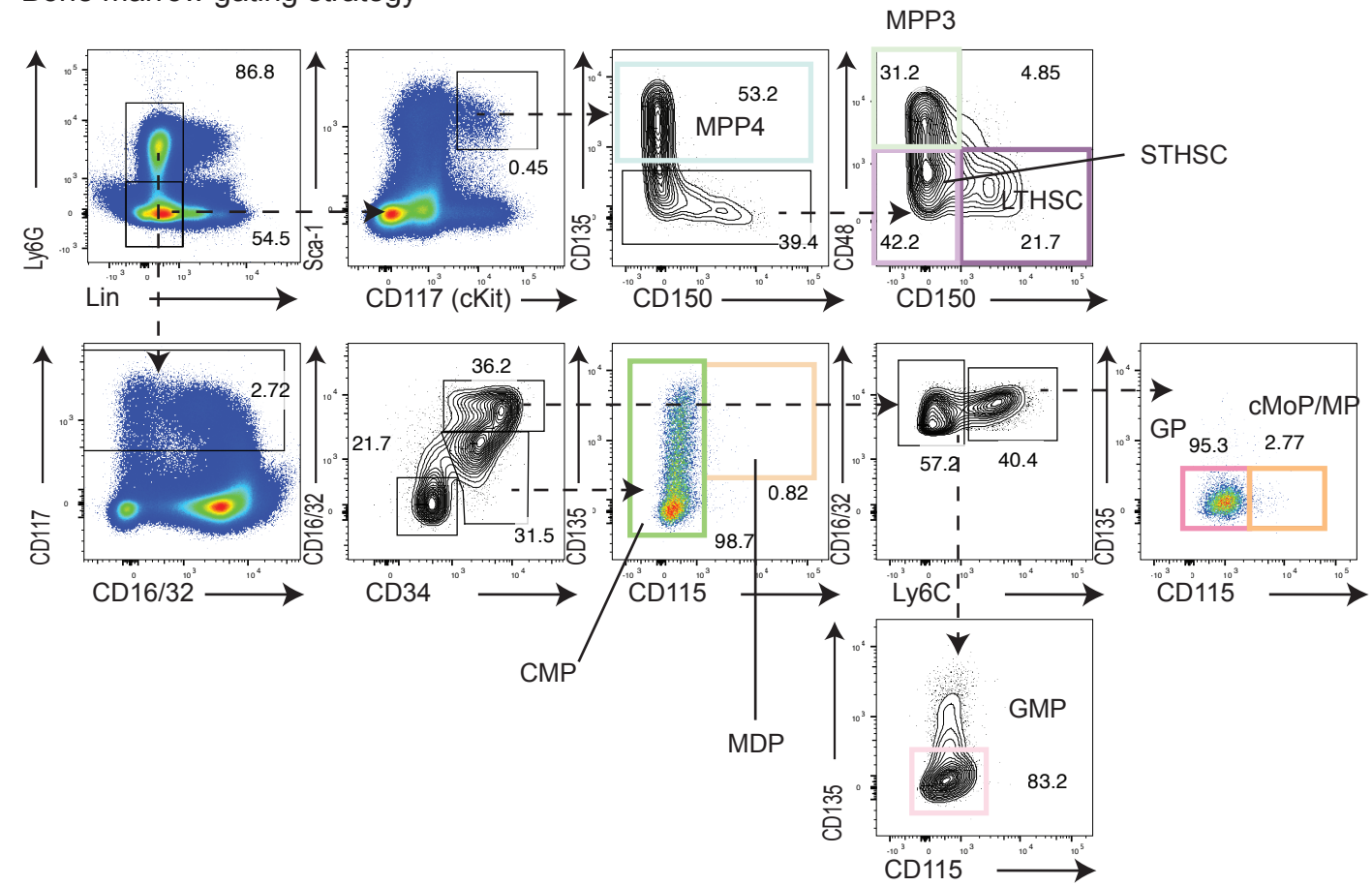

Periphery gating strategy

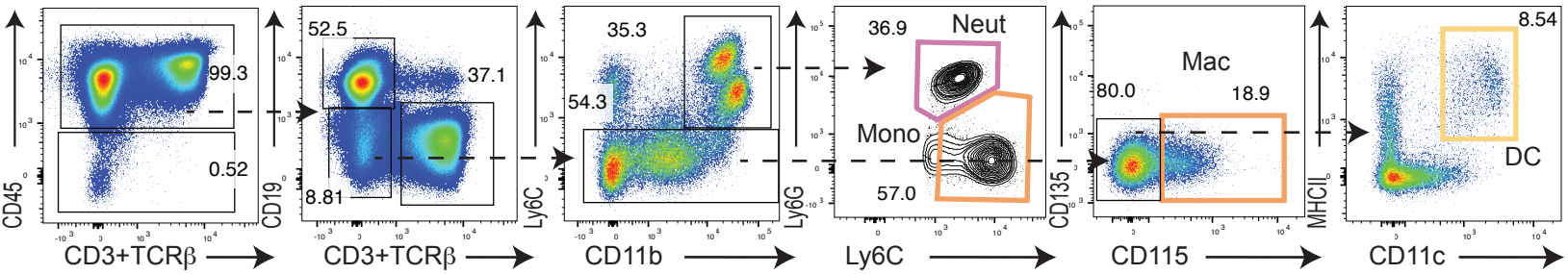

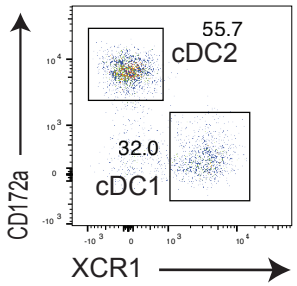

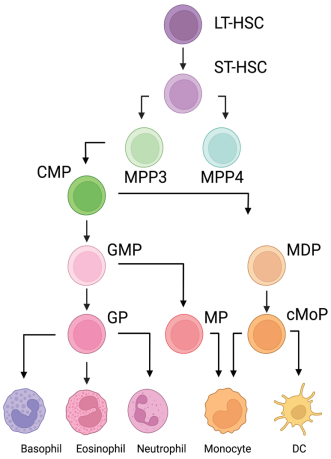

Bone marrow surface markers

Cell Type	Defining Surface Markers
Long-Term Hematopoietic Stem Cell (LTHSC)	Lin (CD3, B220, NK1.1, Ly6G)$^-$, Sca-1$^+$, CD117$^+$, CD135$^-$, CD48$^-$, CD150$^+$
Short-Term Hematopoietic Stem Cell (STHSC)	Lin (CD3, B220, NK1.1, Ly6G)$^-$, Sca-1$^+$, CD117$^+$, CD135$^-$, CD48$^-$, CD150$^-$
Multi-Potent Progenitor 3 (MPP3)	Lin (CD3, B220, NK1.1, Ly6G)$^-$, Sca-1$^+$, CD117$^+$, CD135$^-$, CD48$^+$, CD150$^-$
Multi-Potent Progenitor 4 (MPP4)	Lin (CD3, B220, NK1.1, Ly6G)$^-$, Sca-1$^+$, CD117$^+$, CD135$^+$
Common Myeloid Progenitor (CMP)	(CD3, B220, NK1.1)$^-$, CD117$^+$, CD34$^+$, CD16/32^{lo}, CD115$^-$
Monocyte-Dendritic cell Progenitor (MDP)	(CD3, B220, NK1.1)$^-$, CD117$^+$, CD34$^+$, CD16/32^{lo}, CD115$^+$
Common Monocyte Progenitor (cMoP)/ Monocyte Progenitor (MP)	(CD3, B220, NK1.1)$^-$, CD117$^+$, CD34$^+$, CD16/32^{hi}, Ly6C$^+$, CD135$^-$, CD115$^+$
Granulocyte-Monocyte Progenitor (GMP)	(CD3, B220, NK1.1)$^-$, CD117$^+$, CD34$^+$, CD16/32^{hi}, Ly6C$^-$, CD135$^-$, CD115$^-$
Granulocyte Progenitor (GP)	(CD3, B220, NK1.1)$^-$, CD117$^+$, CD34$^+$, CD16/32^{hi}, Ly6C$^+$, CD135$^-$, CD115$^-$

Periphery surface markers

Cell Type	Defining Surface Markers
T cells	CD45$^+$, CD19$^-$, CD3$^+$, TCRβ$^+$
B cells	CD45$^+$, CD19$^+$, CD3$^-$, TCRβ$^-$
Neutrophils	CD45$^+$, CD19$^-$, CD3$^-$, TCRβ$^-$, CD11b$^+$, Ly6C$^+$, Ly6G$^+$
Monocytes	CD45$^+$, CD19$^-$, CD3$^-$, TCRβ$^-$, CD11b$^+$, Ly6C$^+$, Ly6G$^-$
Macrophages	CD45$^+$, CD19$^-$, CD3$^-$, TCRβ$^-$, Ly6C$^-$, Ly6G$^-$, CD64$^+$
Dendritic Cells	CD45$^+$, CD19$^-$, CD3$^-$, TCRβ$^-$, Ly6C$^-$, Ly6G$^-$, CD64$^-$, CD11c$^+$, MHCII$^+$
Classical Dendritic Cells 1	CD45$^+$, CD19$^-$, CD3$^-$, TCRβ$^-$, Ly6C$^-$, Ly6G$^-$, CD64$^-$, CD11c$^+$, MHCII$^+$, XCR1$^+$, CD172a$^-$
Classical Dendritic Cells 2	CD45$^+$, CD19$^-$, CD3$^-$, TCRβ$^-$, Ly6C$^-$, Ly6G$^-$, CD64$^-$, CD11c$^+$, MHCII$^+$, XCR1$^+$, CD172a$^-$

Figure 2

A.

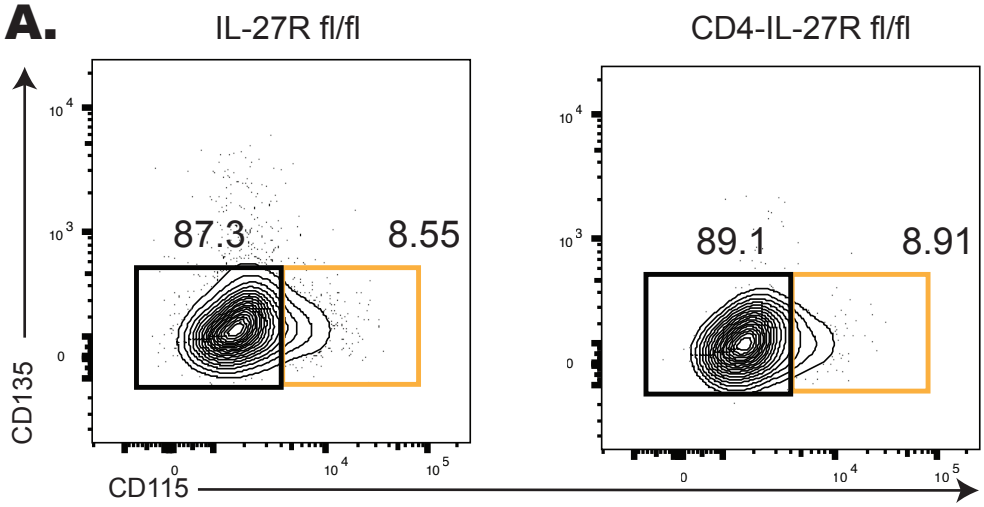

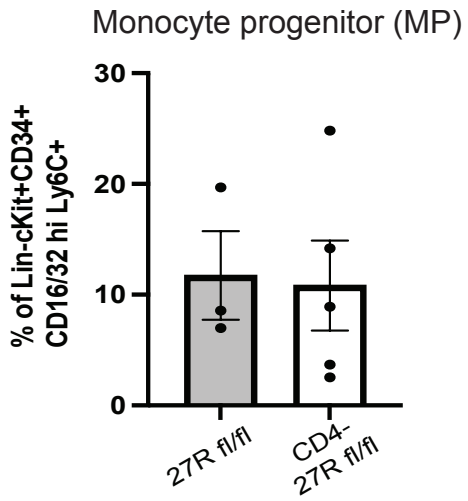

B.

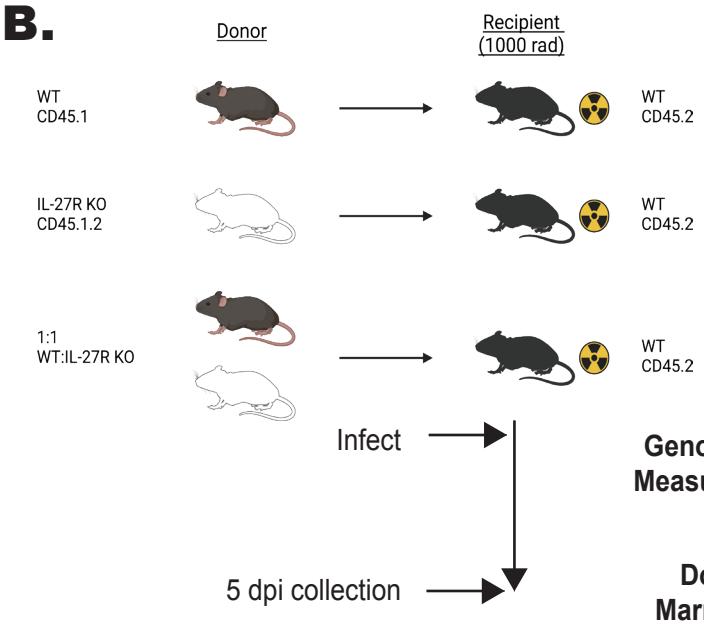

C.

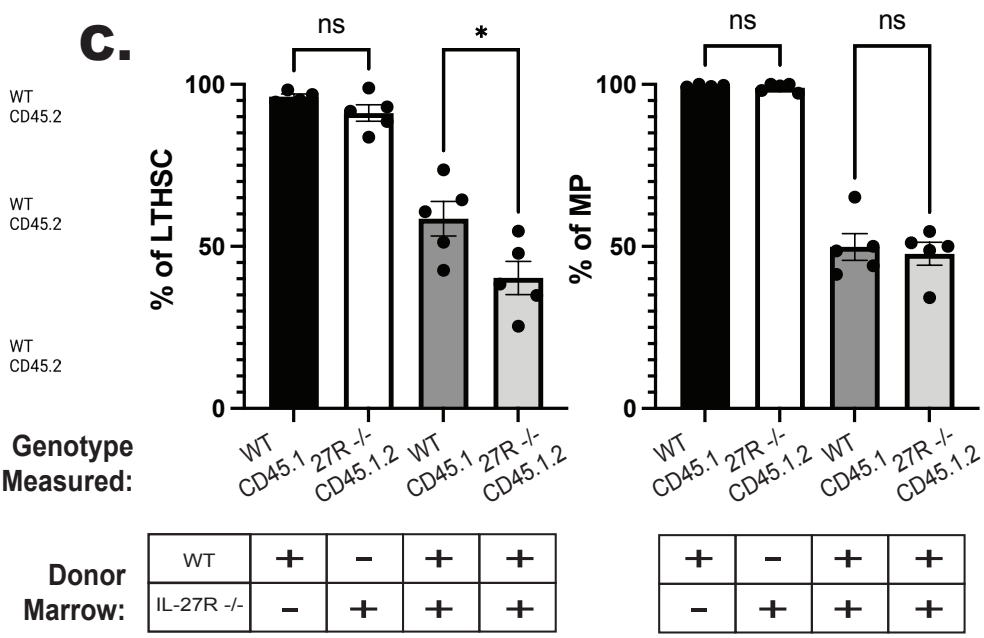

D.

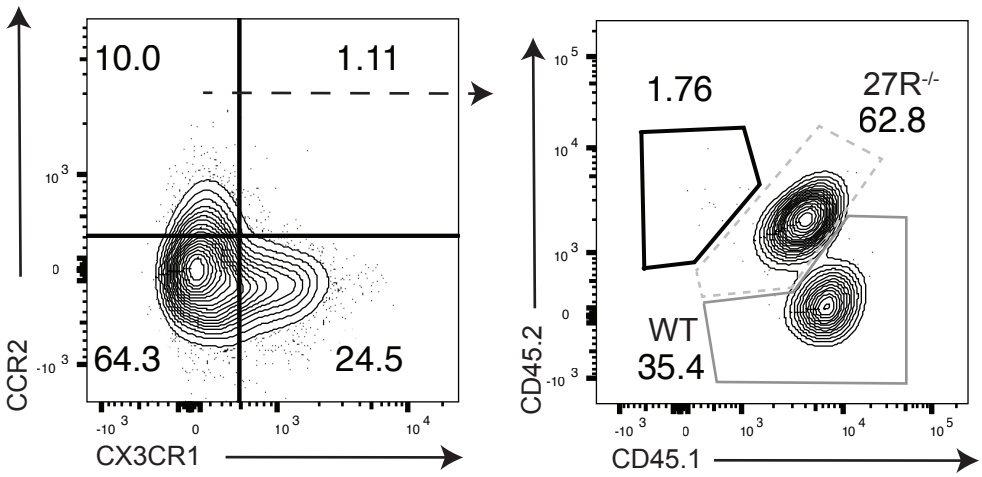

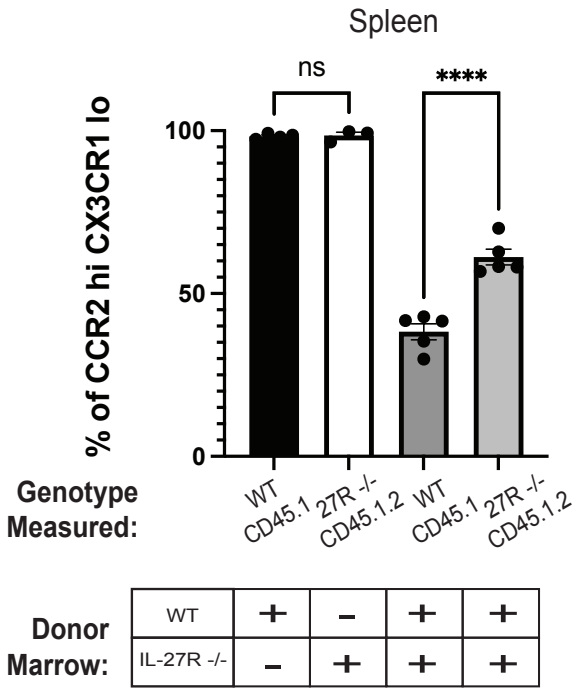

Supplemental Figure 3

A.

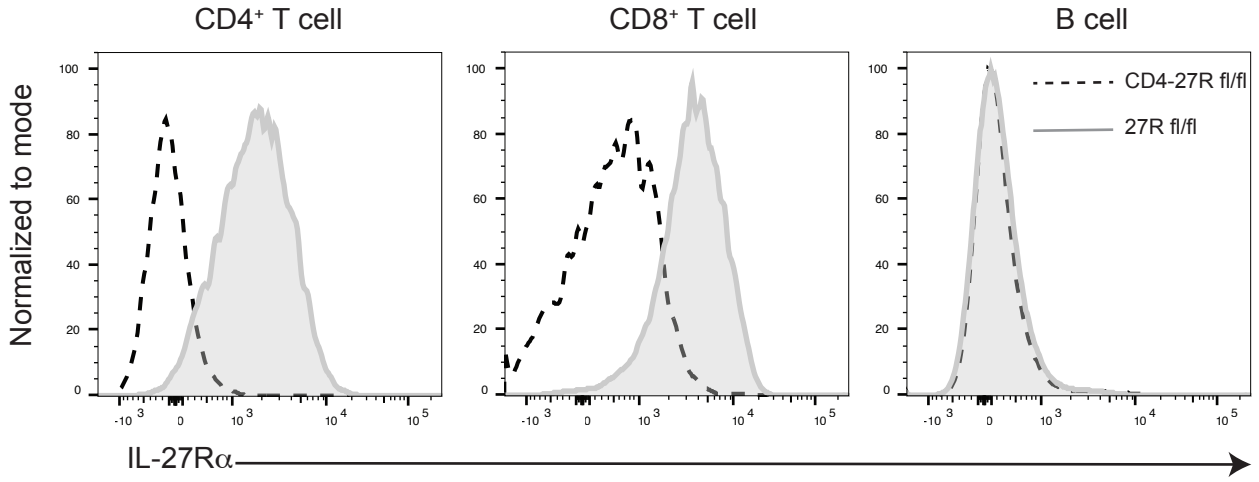

B.

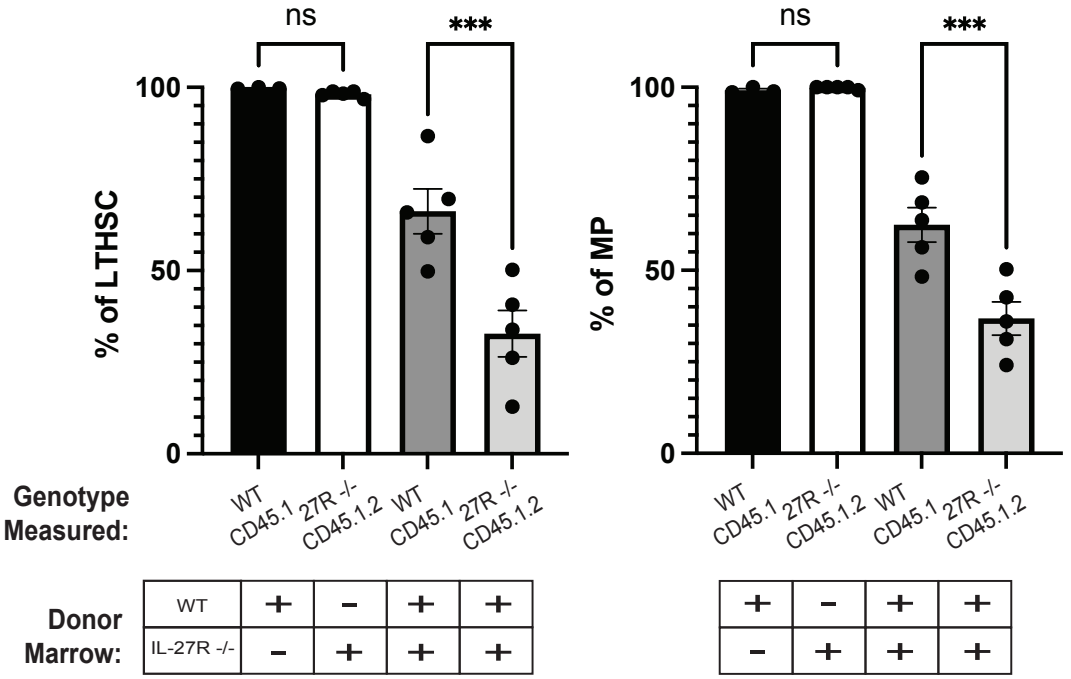

C.

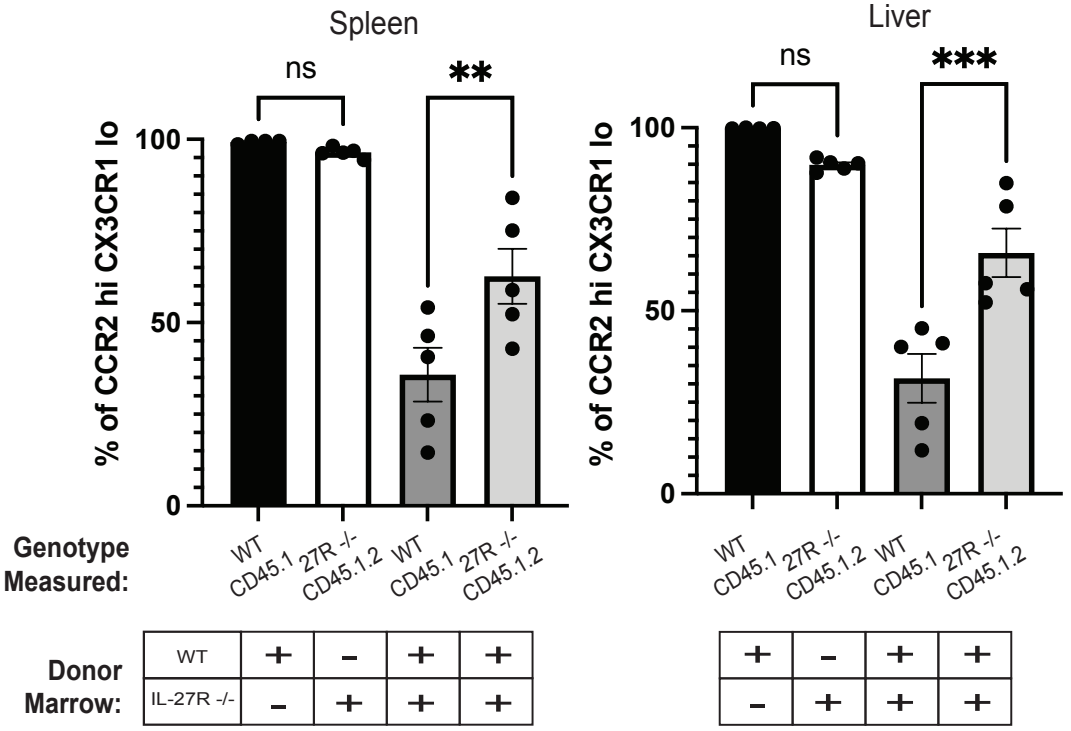

Figure 3

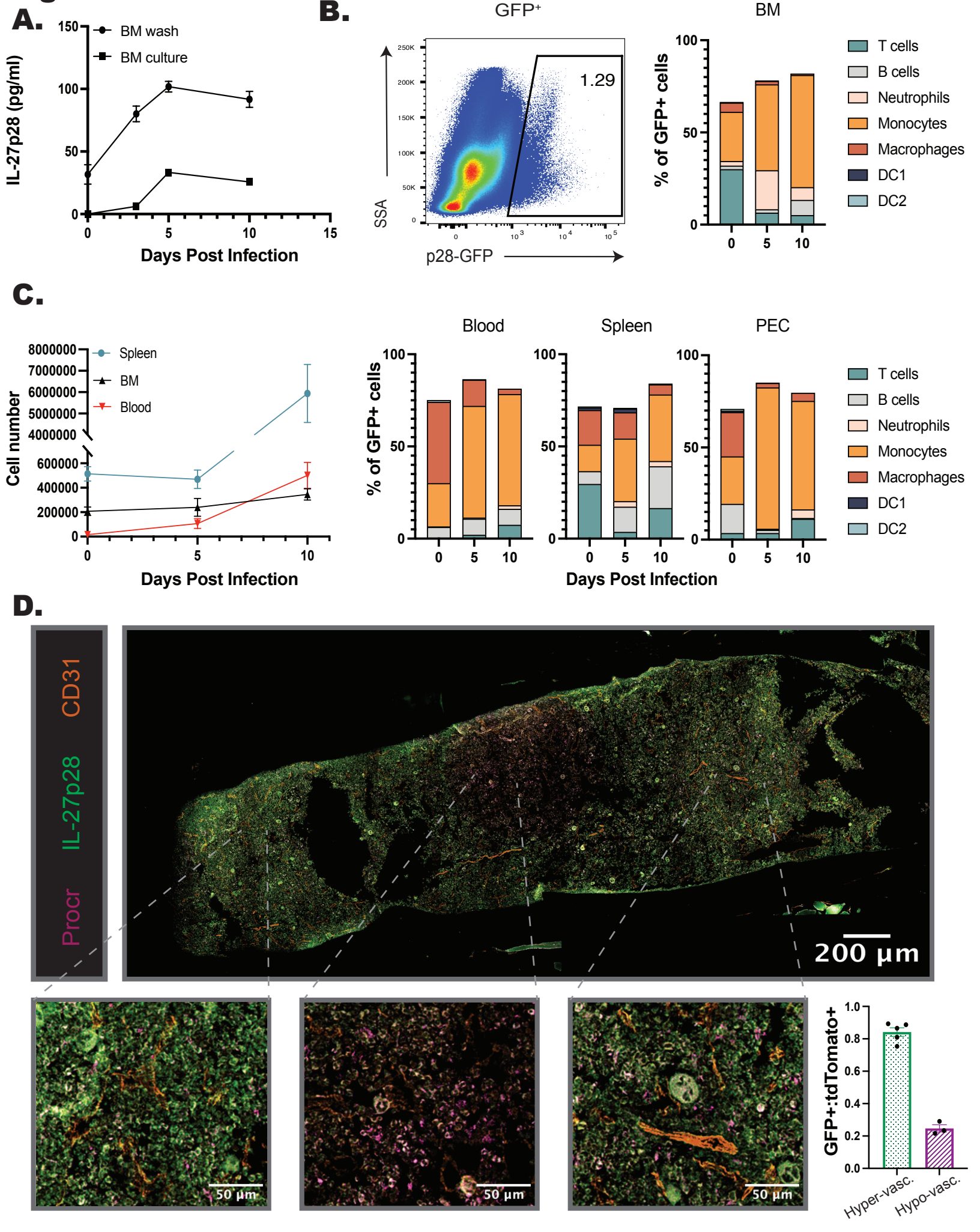
A.
BM wash
BM culture
IL-27p28 (pg/ml)
Days Post Infection
B.
GFP+
BM
1.29
SSA
p28-GFP
% of GFP+ cells
T cells
B cells
Neutrophils
Monocytes
Macrophages
DC1
DC2
C.
Spleen
BM
Blood
Cell number
Days Post Infection
Blood
Spleen
PEC
% of GFP+ cells
Days Post Infection
D.
Procr
IL-27p28
CD31
200 µm
50 µm
50 µm
50 µm
GFP+:tdTomato+
Hyper-vasc.
Hypo-vasc.

Supplemental Figure 4

A.

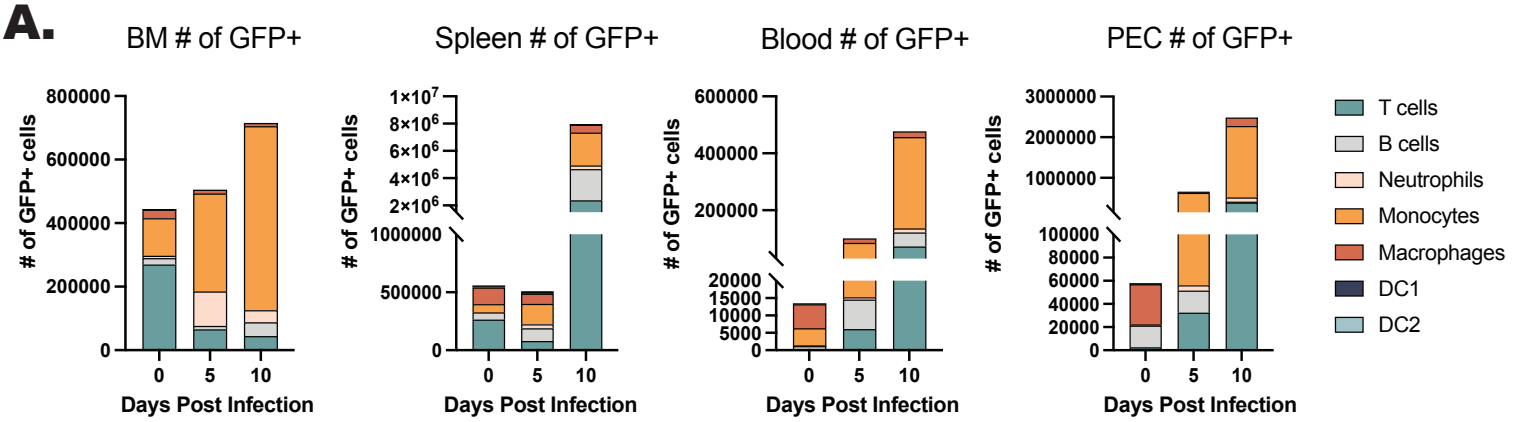

B.

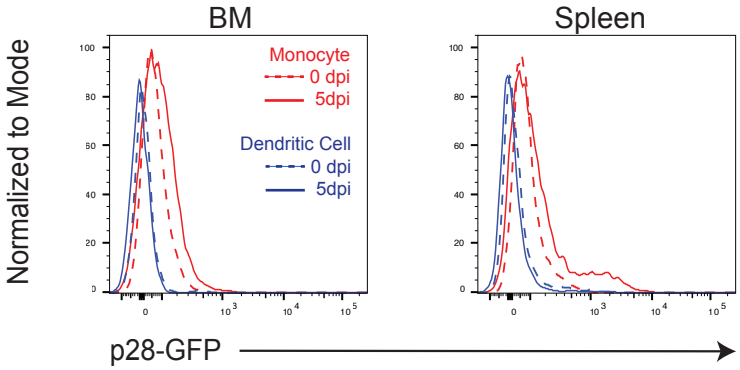

C.

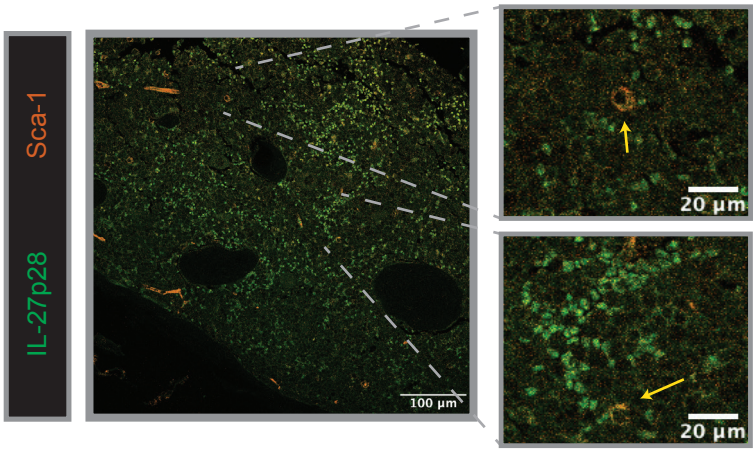

D.

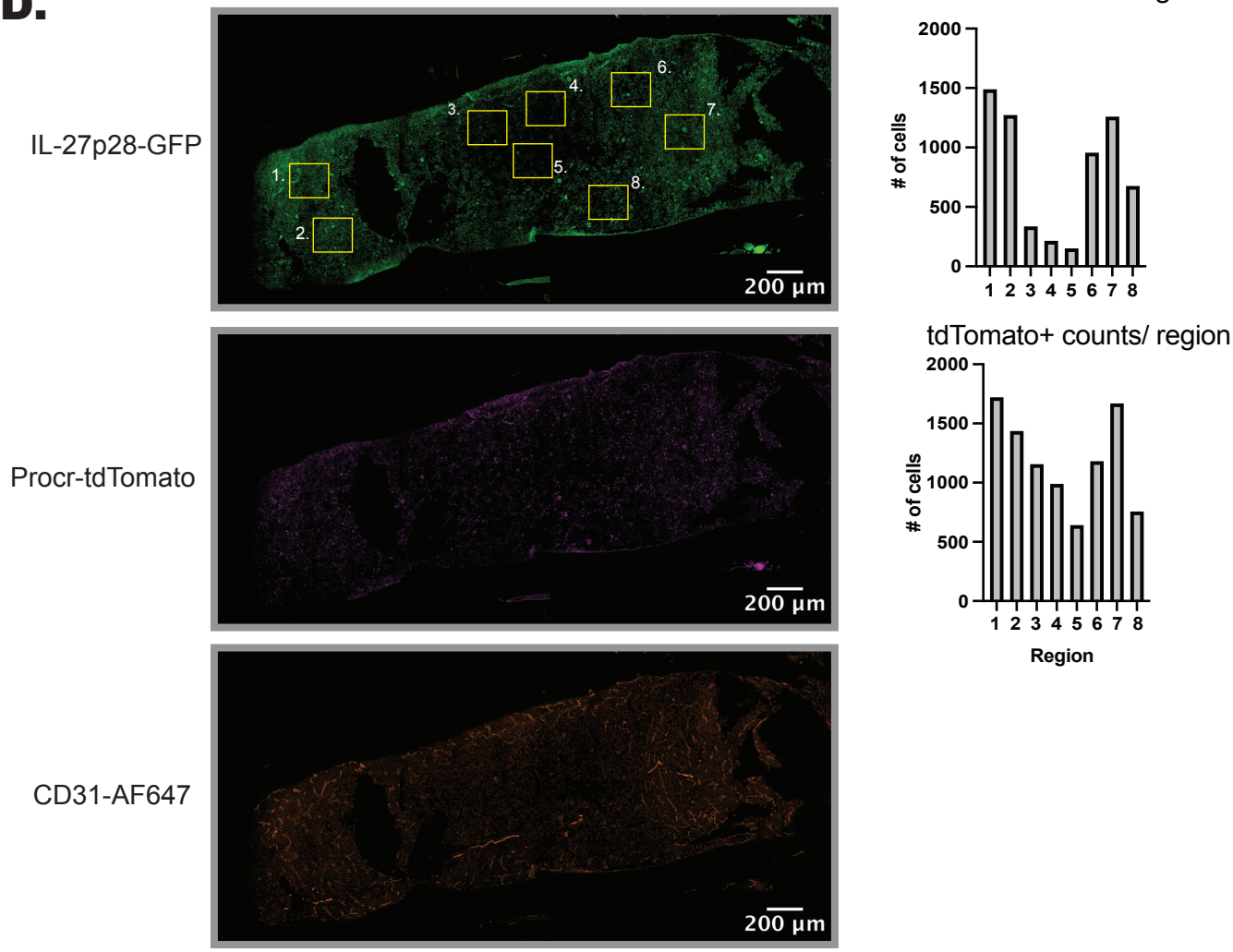

Figure 4

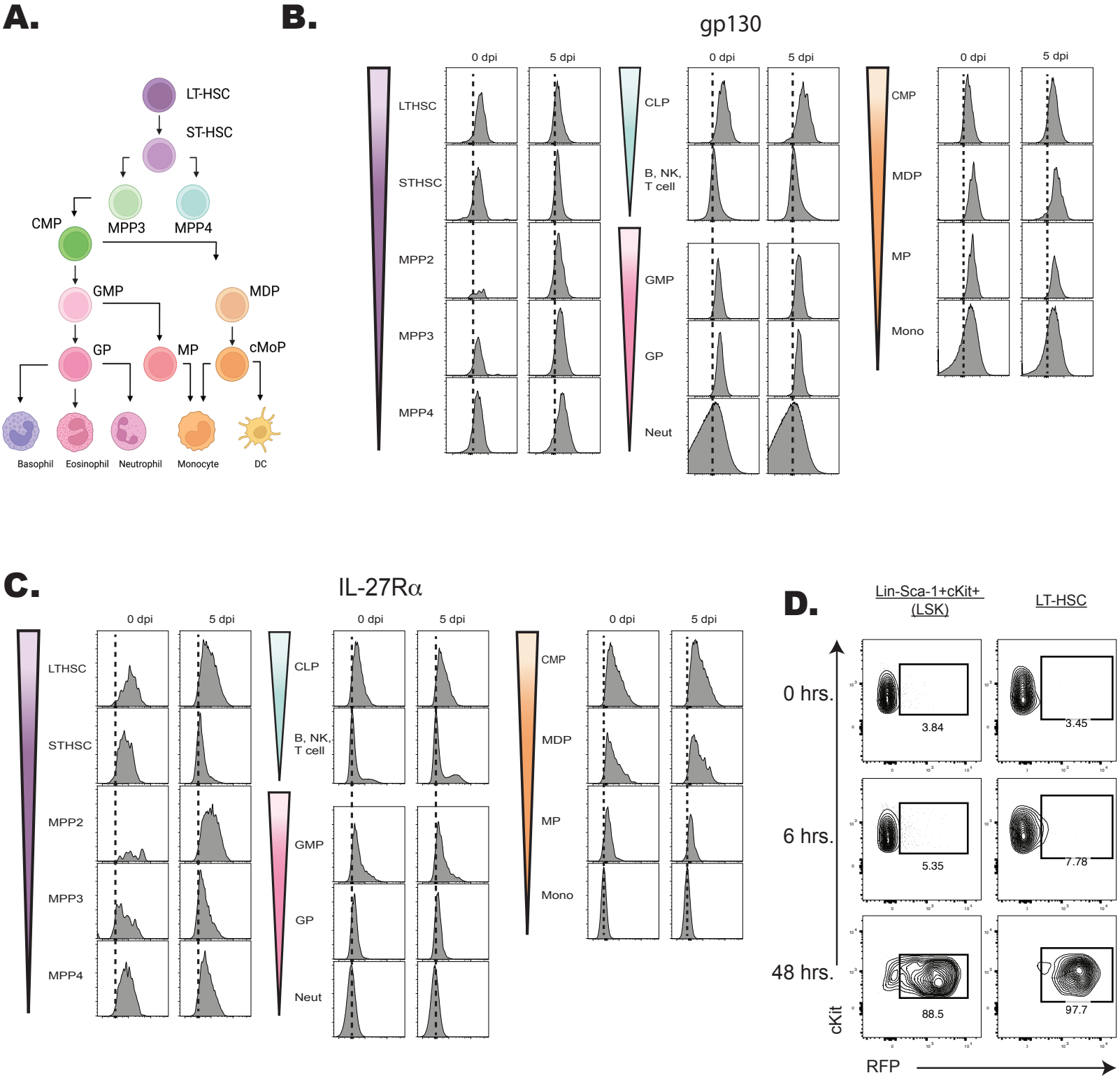
A.
LT-HSC
ST-HSC
CMP
MPP3
MPP4
GMP
MDP
GP
MP
cMoP
Basophil
Eosinophil
Neutrophil
Monocyte
DC
B.
gp130
0 dpi
5 dpi
LTHSC
STHSC
MPP2
MPP3
MPP4
CLP
B, NK, T cell
GMP
GP
Neut
CMP
MDP
MP
Mono
C.
IL-27Rα
0 dpi
5 dpi
LTHSC
STHSC
MPP2
MPP3
MPP4
CLP
B, NK, T cell
GMP
GP
Neut
CMP
MDP
MP
Mono
D.
Lin-Sca-1+cKit+ (LSK)
LT-HSC
0 hrs.
6 hrs.
48 hrs.
3.84
3.45
5.35
7.78
88.5
97.7
cKit
RFP

Supplemental Figure 5

A.

IL27RA expression-Haemosphere

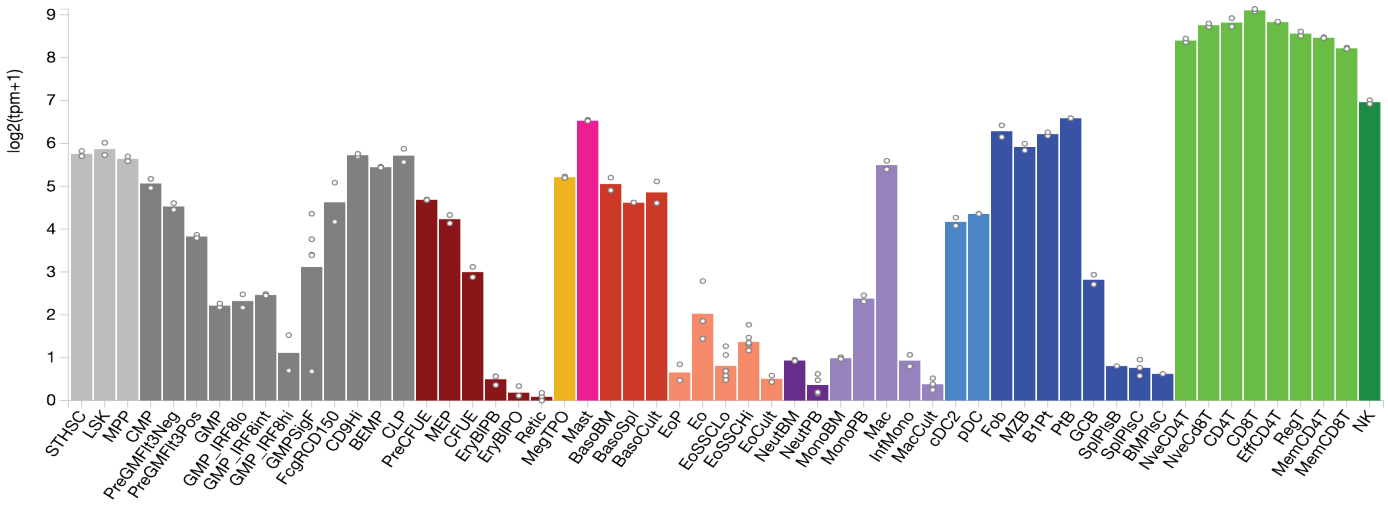

IL27RA expression-BloodSpot

B.

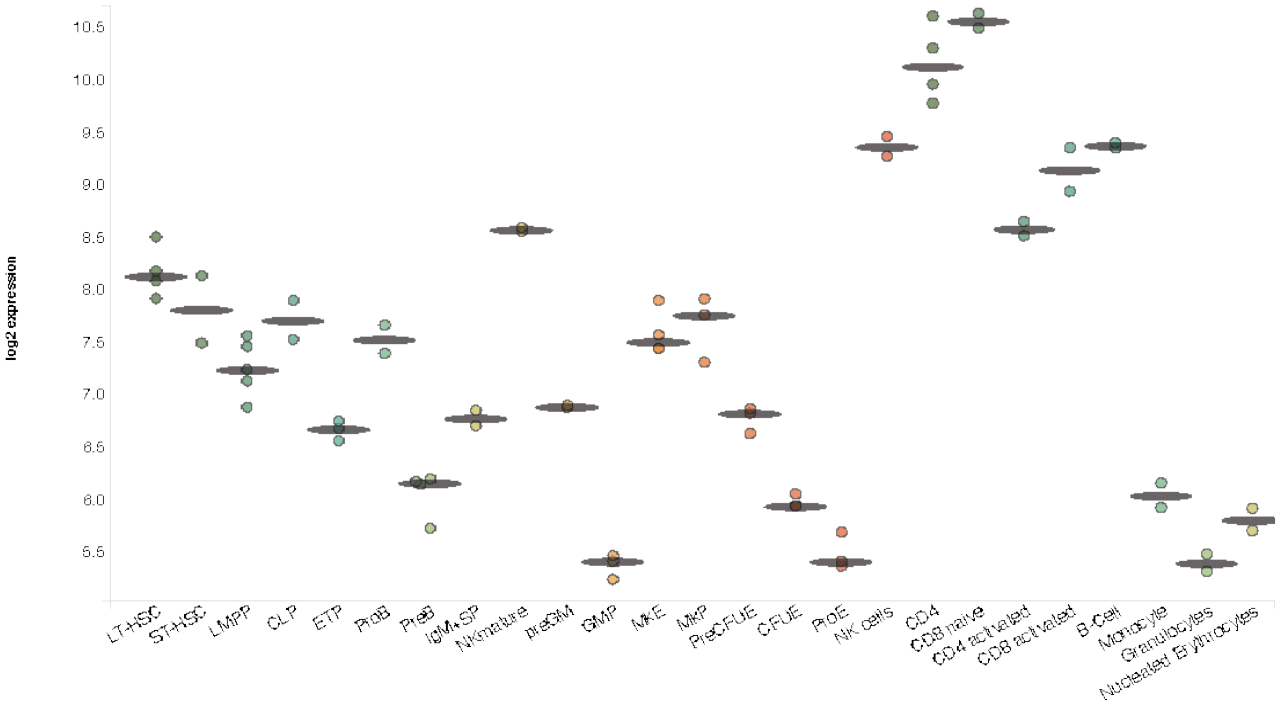

C.

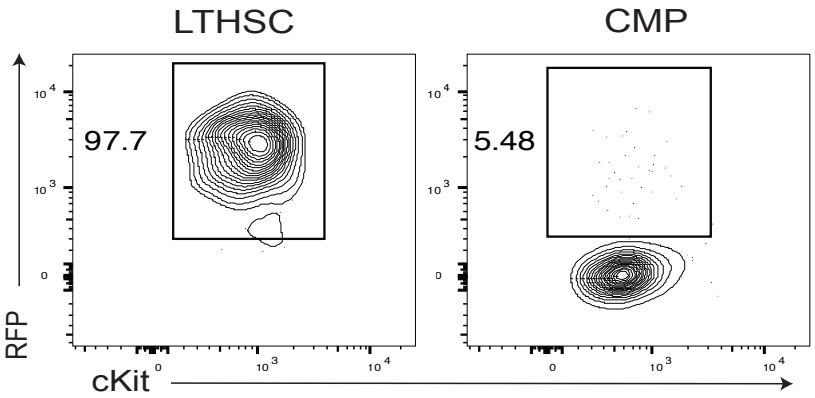

Figure 5

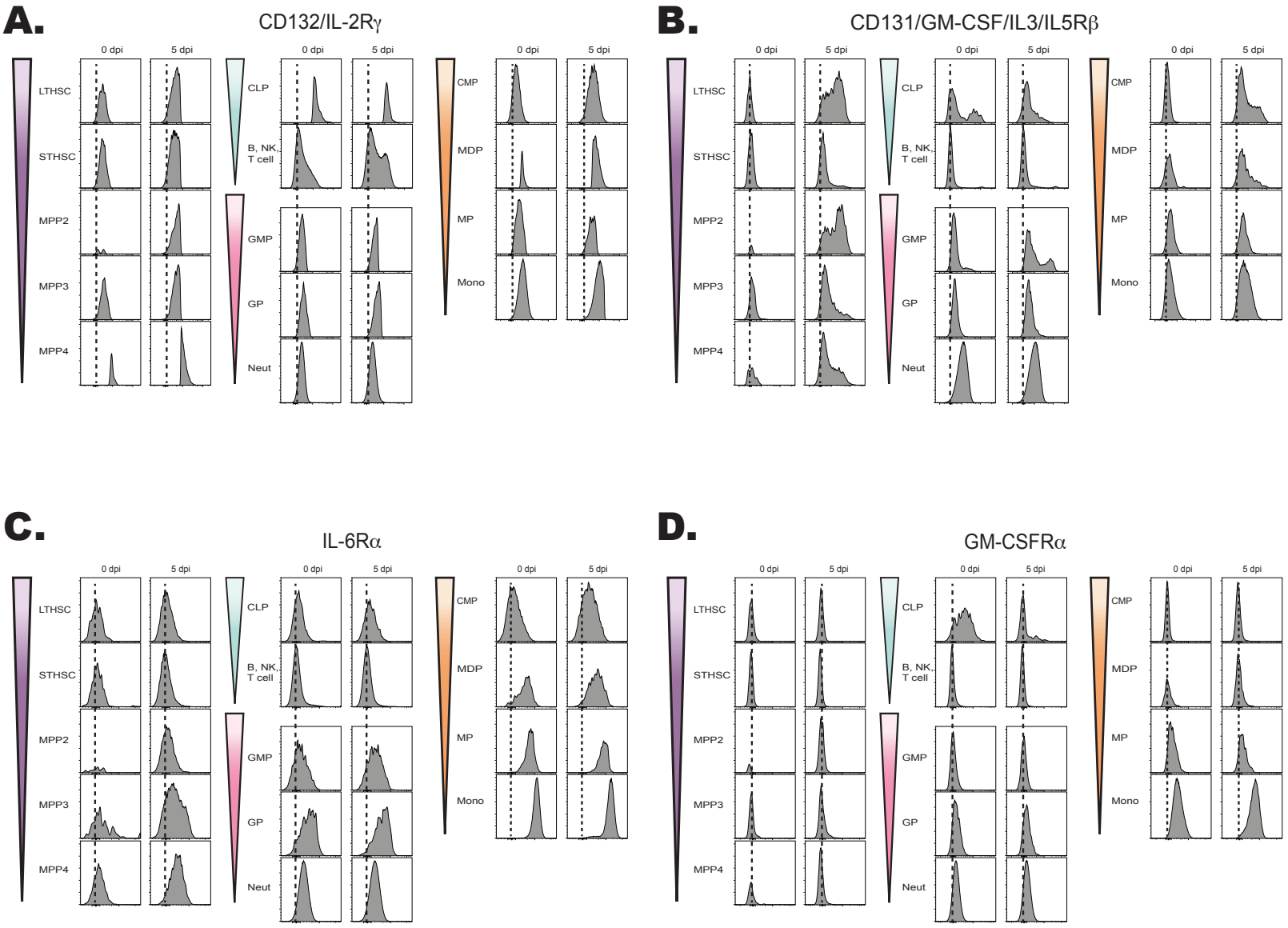
A.
CD132/IL-2Rγ
B.
CD131/GM-CSF/IL3/IL5Rβ
C.
IL-6Rα
D.
GM-CSFRα
0 dpi
5 dpi
LTHSC
STHSC
MPP2
MPP3
MPP4
CLP
B, NK, T cell
GMP
GP
Neut
CMP
MDP
MP
Mono

Supplemental Figure 6

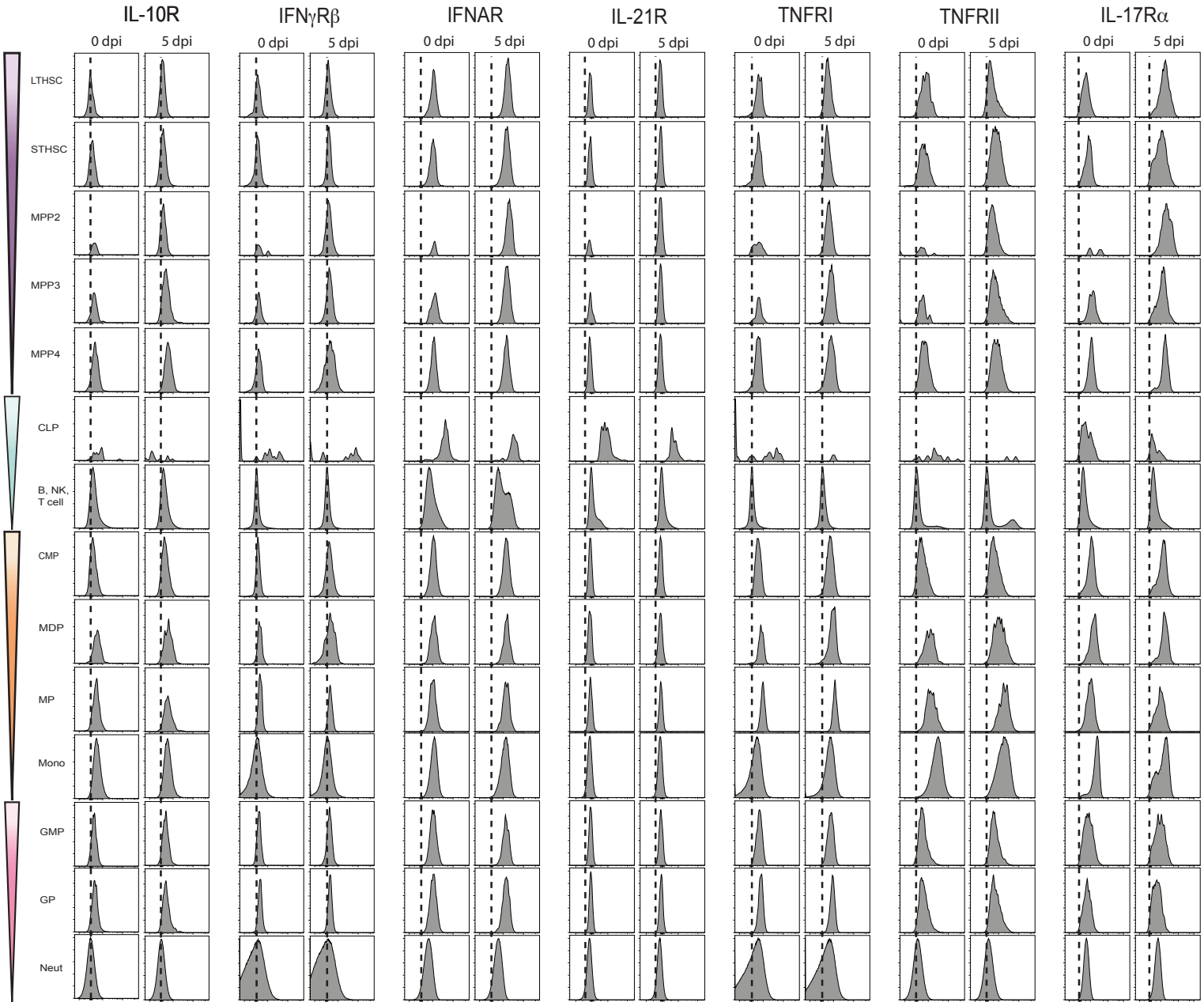

Figure 6

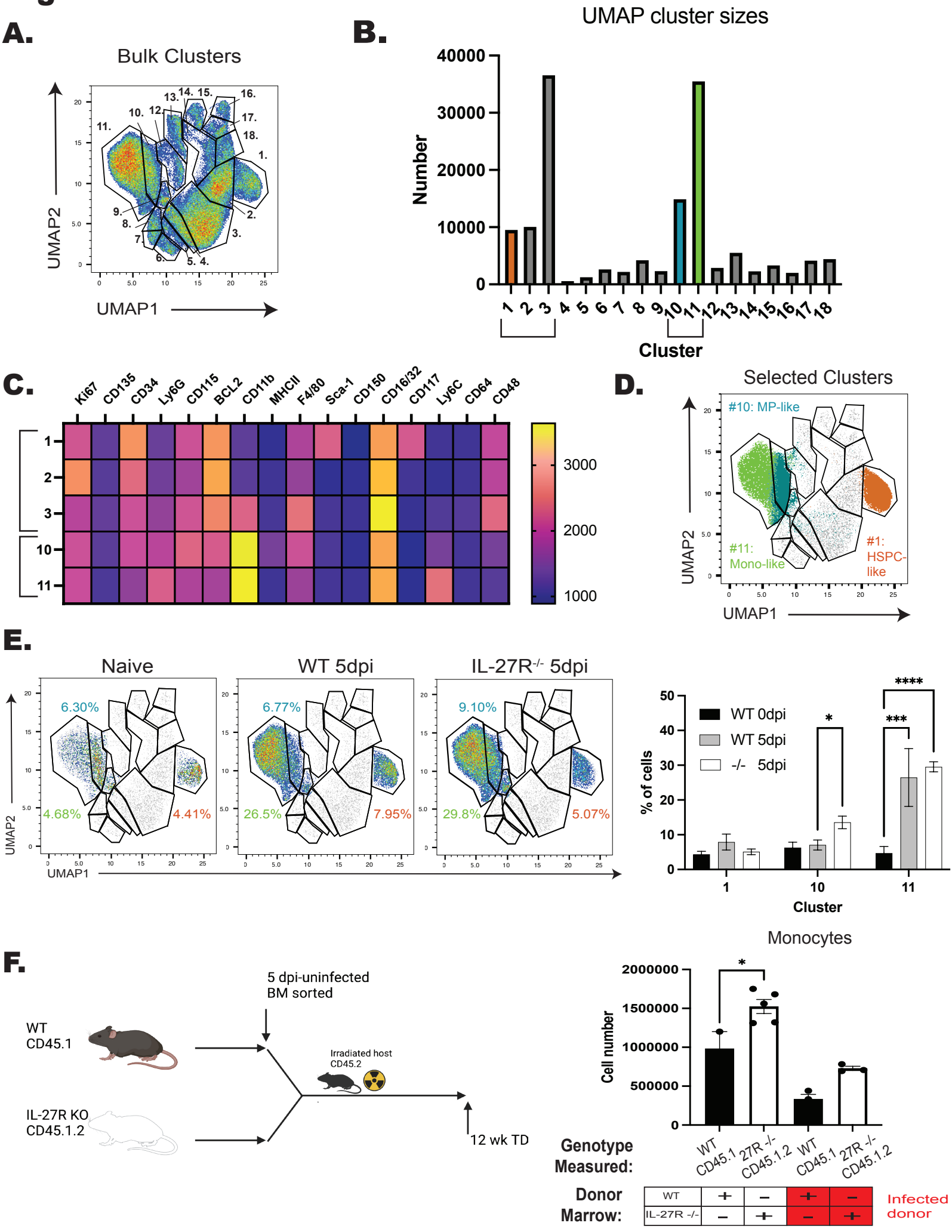
A.
Bulk Clusters
UMAP2
UMAP1
B.
UMAP cluster sizes
Number
Cluster
C.
Ki67
CD135
CD34
Ly6G
CD115
BCL2
CD11b
MHCII
F4/80
Sca-1
CD150
CD16/32
CD117
Ly6C
CD64
CD48
D.
Selected Clusters
#10: MP-like
#11: Mono-like
#1: HSPC-like
UMAP2
UMAP1
E.
Naive
WT 5dpi
IL-27R-/- 5dpi
6.30%
4.68%
4.41%
6.77%
26.5%
7.95%
9.10%
29.8%
5.07%
UMAP2
UMAP1
WT 0dpi
WT 5dpi
-/- 5dpi
% of cells
Cluster
F.
5 dpi-uninfected BM sorted
WT CD45.1
IL-27R KO CD45.1.2
Irradiated host CD45.2
12 wk TD
Monocytes
Cell number
Genotype Measured:
WT CD45.1
27R -/- CD45.1.2
Donor Marrow:
WT
IL-27R -/-
Infected donor

Supplemental Figure 7

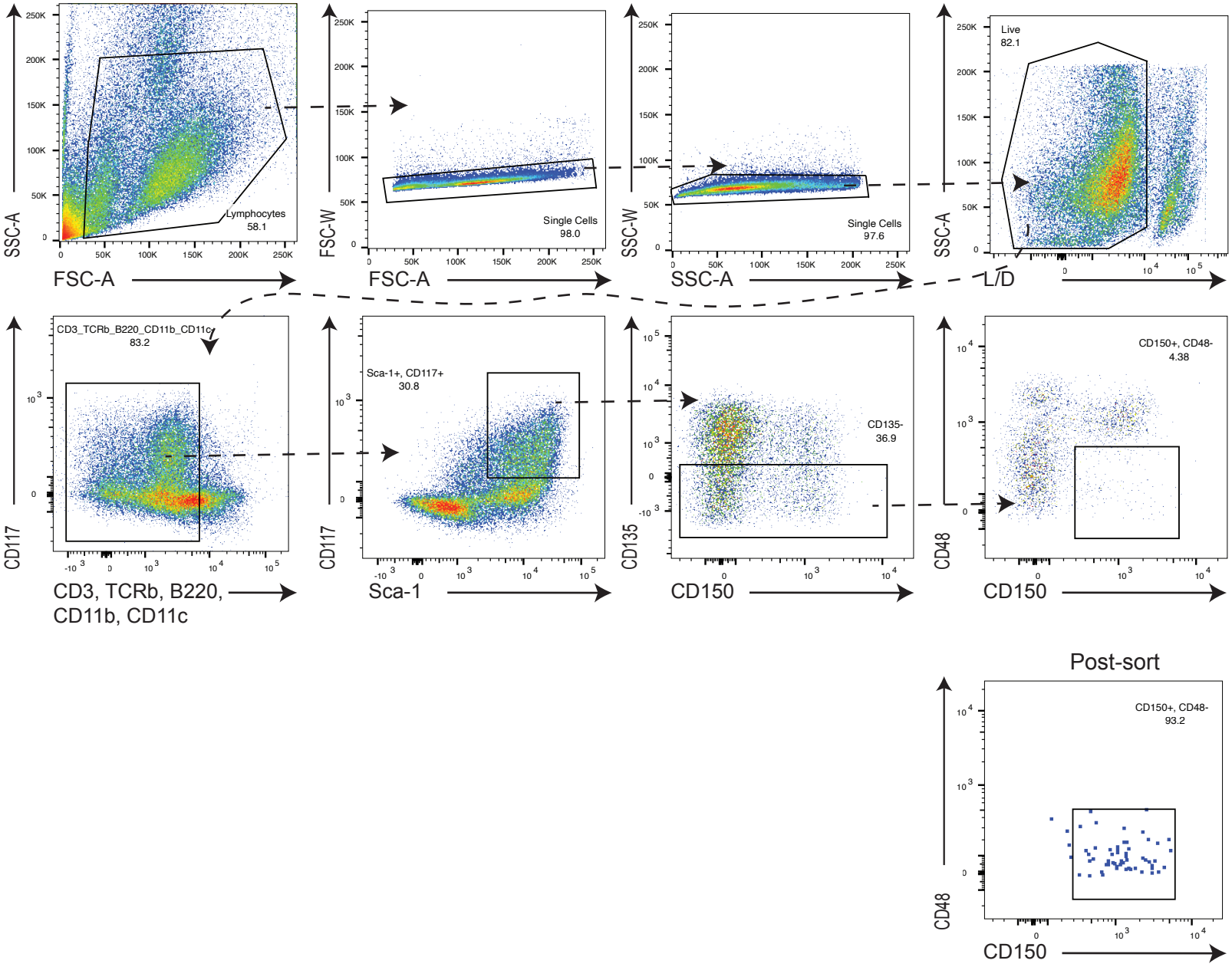

Supplemental Figure 8

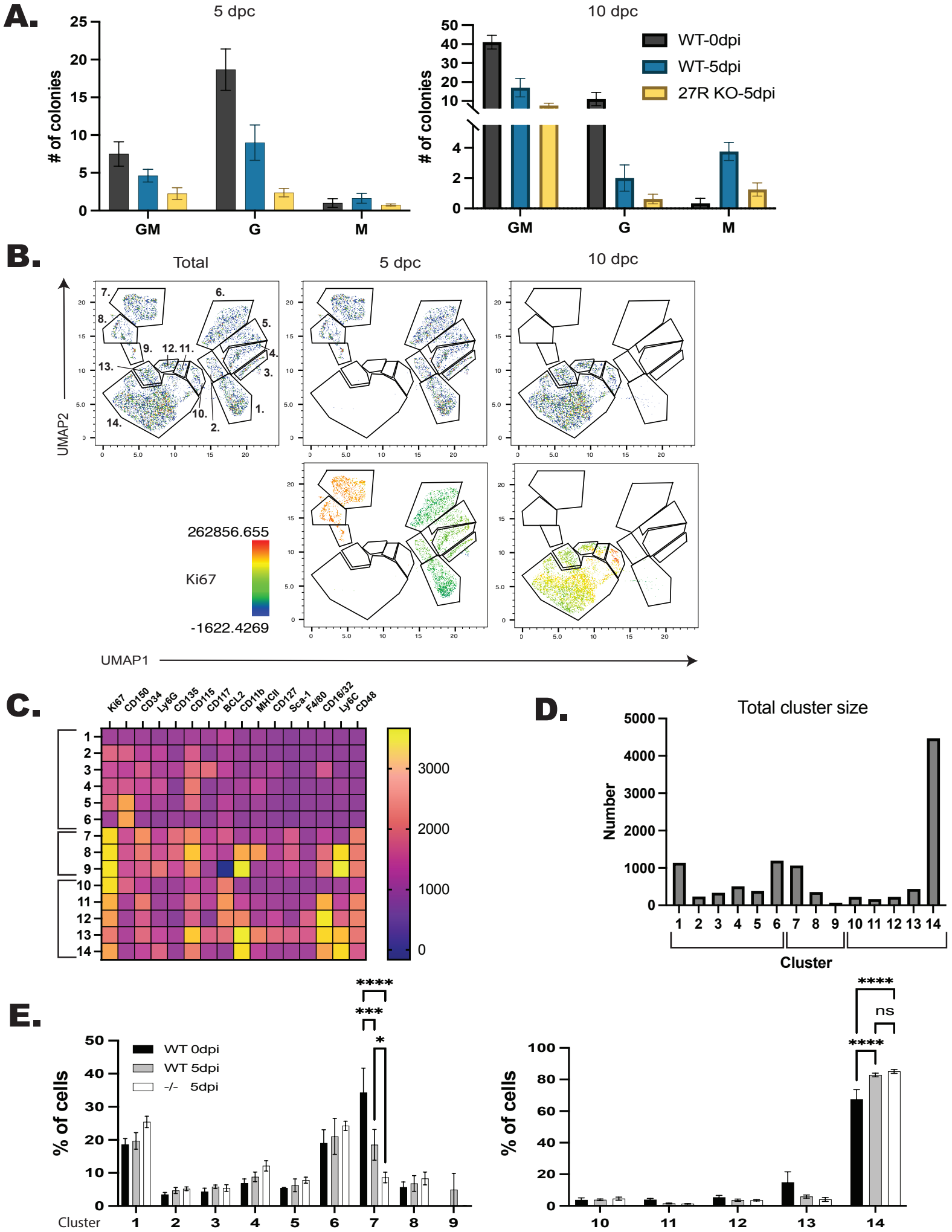

Figure 7

A.

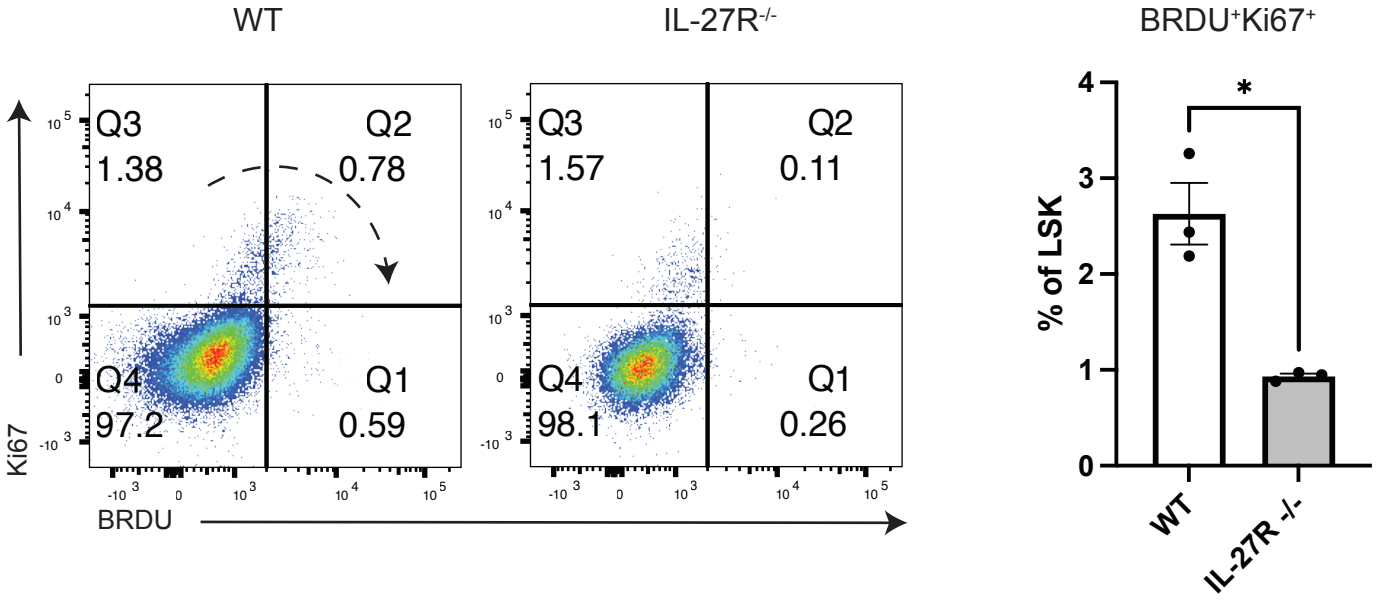

B.

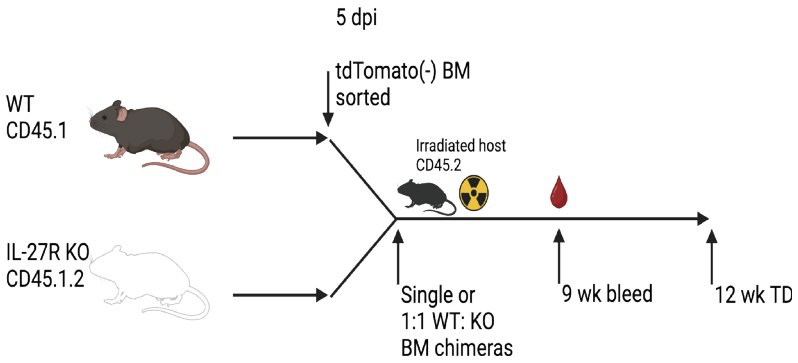

C.

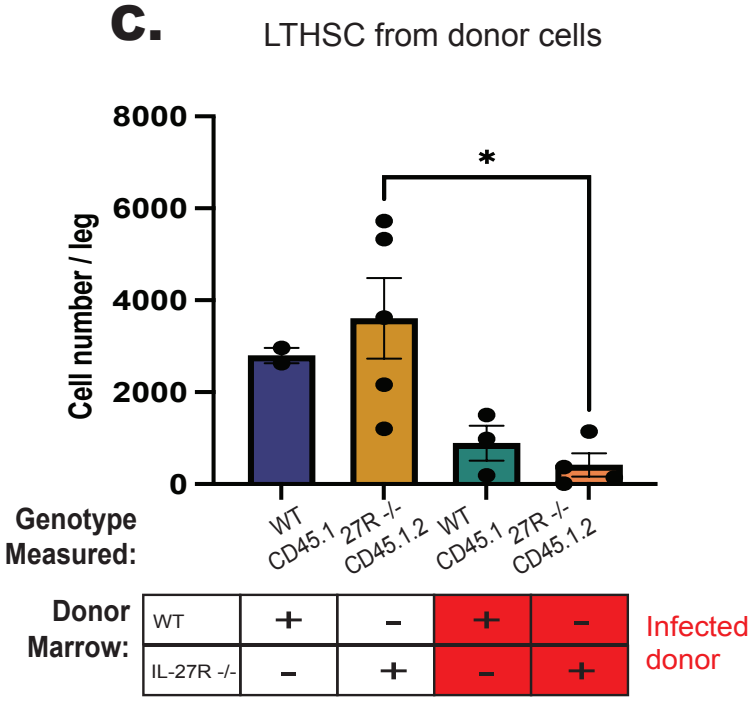

D.

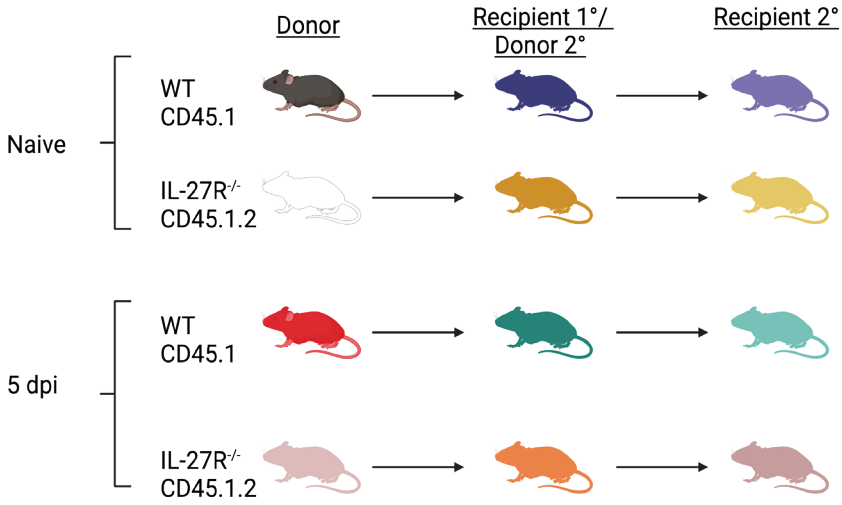

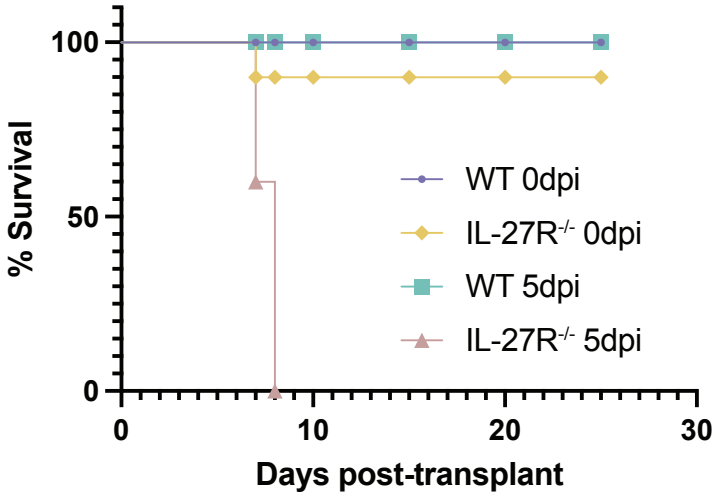

Supplemental Figure 9

A.

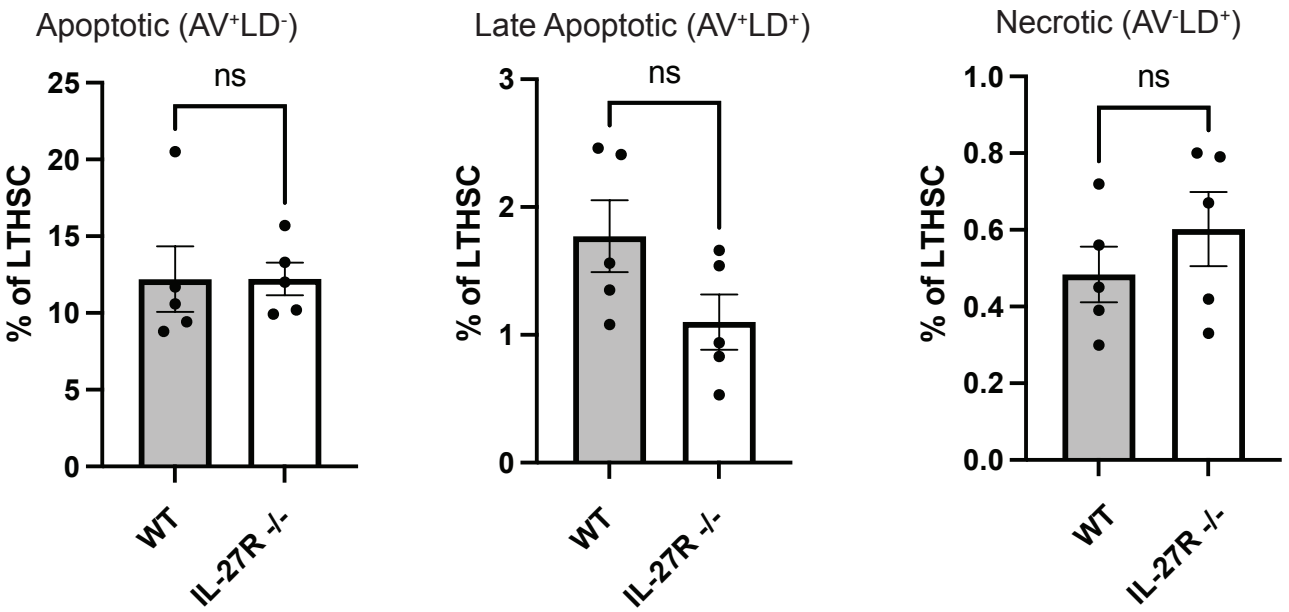
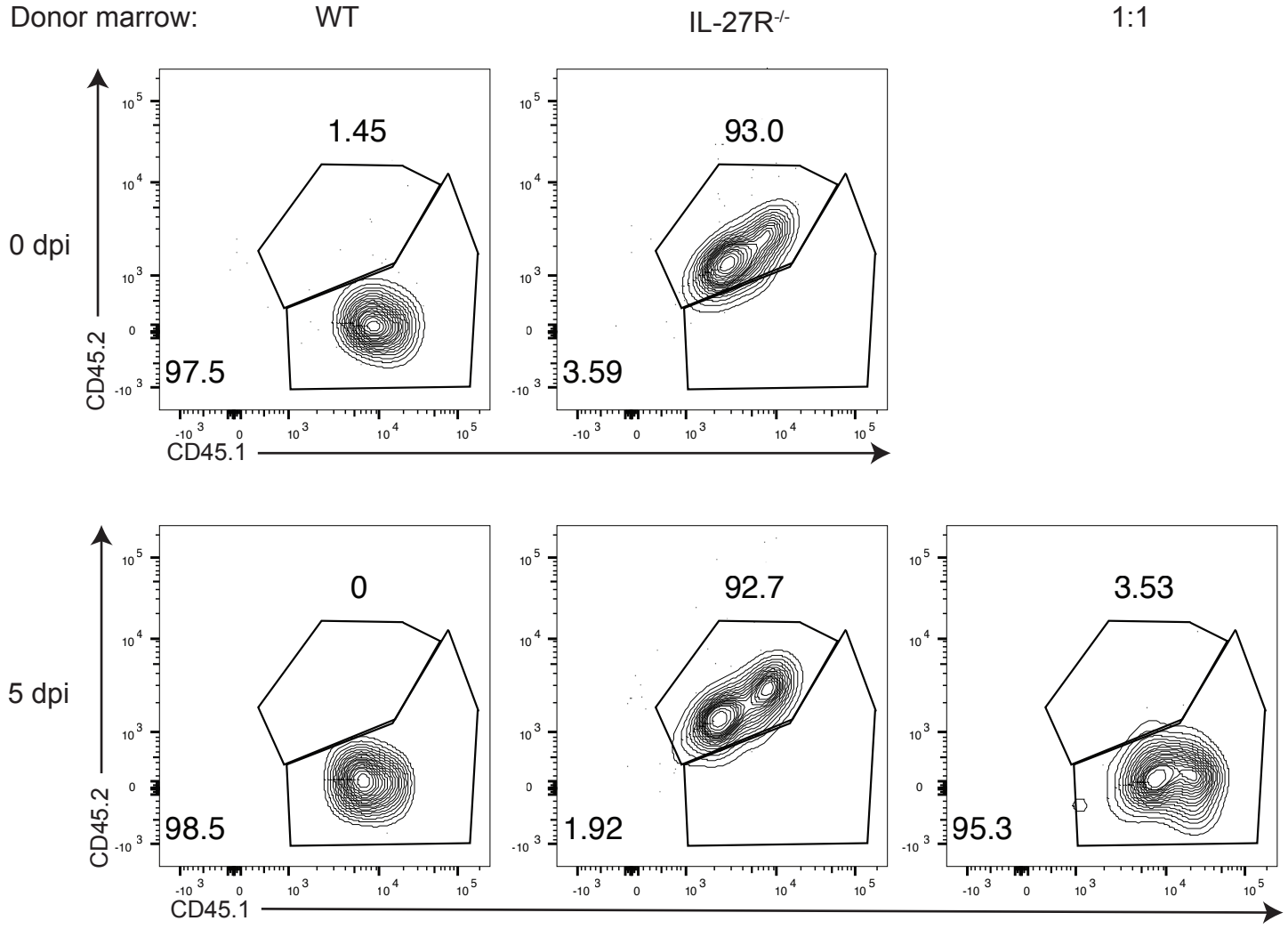
B.